Impact of regolith thickness on regional seismic amplification

Hafiz Imtenan Elahi

February, 2009

Impact of regolith thickness on regional seismic amplification

By

Hafiz Imtenan Elahi

Thesis submitted to the International Institute for Geo-information Science and Earth Observation in partial fulfilment of the requirements for the degree of Master of Science in Geo-information Science and Earth Observation, Specialisation: (Geo-engineering)

Thesis Assessment Board

Prof. Dr. F.D. van der Meer (Chairman)
Prof. Dr. J. van der Kruk (External Examiner)
Dr. M. van der Meijde (First Supervisor)
Prof. Dr. F.D. van der Meer (Second Supervisor)
Muhammad Shafique (PhD scholar, Advisor)
Drs. T.M. Loran (Course Director, AES)

ITC

INTERNATIONAL INSTITUTE FOR GEO-INFORMATION SCIENCE AND EARTH OBSERVATION
ENSCHEDE, THE NETHERLANDS

Disclaimer

This document describes work undertaken as part of a programme of study at the International Institute for Geo-information Science and Earth Observation. All views and opinions expressed therein remain the sole responsibility of the author, and do not necessarily represent those of the institute.

Dedicated to my father
Whom I lost during the course of this study

Abstract

Influence of regolith thickness on the variance of seismic ground shaking is widely accepted. However most of the studies assume it constant for simplicity. Regolith thickness can be modelled by integrating field observations, geology and topography using GIS and geostatistical tools. A predicted thickness of regolith map can be used for assessing seismic amplification. The present study was conducted in the seismically active area of Balakot and Muzaffarabad in Pakistan administered Kashmir region. Regolith thickness was determined by field measurements carried out on the exposed outcrops and modelled by integrating with geology, slope and elevation using GIS and geostatistical tools. ASTER (Advanced Spaceborne Thermal Emission and Reflection Radiometer) and SRTM (Shuttle Radar Topography Mission) digital elevation models (DEMs) were used for deriving slope and elevation and modelling regolith thickness. A site condition map based on geology and shear wave velocity was prepared for the assessment of seismic amplification. The predicted regolith thickness in the study area varies from 1 to 10 meters. Slope, geology, and elevation have influence on regolith thickness and their correlation coefficients with regolith thickness are -0.43, 0.36 and -0.28 respectively with slope and elevation derived from ASTER DEM. Correlation coefficients of regolith thickness with slope and elevation derived from SRTM DEM are -0.48 and -0.27 respectively. The adjusted R-square and p-values of model derived from ASTER DEM are 0.20 and $5.7e^{-08}$ respectively, whereas that derived from SRTM DEM are 0.14 and $1.6e^{-05}$ respectively. The study concluded that regolith thickness is more in the centre of the valleys, flatter slopes and the areas where soft rocks are exposed. The model derived from ASTER DEM explains more variation and is more significant then that of SRTM DEM. More observations for the regolith thickness can be useful for further study.

Keywords: Regolith thickness, slope, elevation, geology, seismic ground shaking, Balakot, Muzaffarabad.

Acknowledgements

At the completion of this thesis, first of all I am grateful to God who provided me this opportunity for this degree and created people who helped me in this regard.
I express my gratitude to NFP and ITC for their support in the present study and my organization GSP (Geological Survey of Pakistan) for nominating me for this course. Special thanks go to Mr. Mark van der Meijde for his support in formulating the research topic, for his patience and wisdom in supervising me. I am extremely grateful to Mr. Freek van der Meer, my second supervisor for his precious criticism and support during the work. I am highly indebted to the PhD scholar Muhammad Shafique for his constructive and valuable suggestions in carrying out this work.
I extend my gratitude to the Centre of Excellence in Geology, Department of University of Peshawar for their support in the field work and all the organizations that provided data for this work.
Finally I would like to express my deep respect and appreciation for my family in providing me moral support in this period of study.

Hafiz Imtenan Elahi
Enschede, The Netherlands.
February, 2009.

Table of contents

1. Introduction 7
1.1. Background 7
1.2. Research problem 8
1.3. Research objective 9
1.4. Sub objectives 9
1.5. Research questions 9
1.6. Research hypothesis 9
1.7. Literature review 9
1.7.1 Factors affecting the ground seismic response 9
1.7.2 Impact of thickness of regolith 11
1.7.3 Impact of geology 11
1.7.4 Impact of topography 11
2. Study Area 13
2.1. Seismicity 14
2.2. Geological and geomorphic setting of the study area 14
3. Material and methods 18
3.1. Methodology 18
3.2. Pre field work acitivty 19
3.3. Field data collection 19
3.4. Derivation of terrain attributes from the DEMs 21
3.4.1. Comparison of Elevations 21
3.4.2. Comparison of slopes 22
3.4.3. Modelling thickness of regolith 24
3.5. Construction of site condition map 26
4. Results and discussion 28
4.4. Relationships between thickness of regolith and geology. 28
4.5. Relationships between regolith thickness and topographic attributes. 32
4.5.1. Relationships of thickness of the unconsolidated material and slope 32
4.5.2. Relationships of thickness of the unconsolidated material and elevation 36
4.6. Maps of thickness of regolith 39
4.7. Site condition map 44
4.8. Chapter of ground penetrating radar 42
5. Conclusions and recommendations 43
5.4. Concusions 43
5.5. Recommendations 43
5.6. Limitations 44
Appendix 1 50
6. Results of ground penetrating radar 48
6.1. Introduction 48
6.2. GPR theory 49
6.3. GPR application 51
6.4. Data processing 51

6.5. GPR application in delineating regolith boundary……………………………………………51

List of figures

Figure 1 Variance of seismic waves due to the unconsolidated material.. 8
Figure 2 Framework of seismic shaking prediction, Source: (Shafique, 2008) 10
Figure 3 Factors responsible for the seismic ground shaking, Source: (Shafique et al., 2008) 10
Figure 4 Location of the study area... 13
Figure 5 Large earthquakes along Himalaya region (from Wright 2005) 14
Figure 6 Geological map of the study area 17
Figure 7 Flow chart of the research approach.. 18
Figure 8 Bedrock regolith boundary exposed in Muzaffarabad - Balakot Area 20
Figure 9 Outcrop observations (yellow dots) on ASTER image of the study area 20
Figure 10 Correlations of GPS elevation and ASTER (a), GPS and SRTM DEM (b) and between ASTER and SRTM DEMs (c) 22
Figure 11 Correlations of slopes derived from field and ASTER (a), field and SRTM DEM (b) and ASTER and SRTM DEMs (c).. 23
Figure 12 Correlation between Geology and thickness.. 28
Figure 13 Thickness and geology with variation in slope and elevation of ASTER (a) and (c) and SRTM (b) and (d) respectively 29
Figure 14 Geology predicted thickness of regolith map.. 31
Figure 15 Correlation between thickness of regolith and slope of ASTER (left) and SRTM DEMs (right) 32
Figure 16 Thickness of regolith and slope with variation in elevation of ASTER (a) and SRTM DEMs (b) and geology (c) and (d)... 33
Figure 17 Slope predicted thickness of regolith map (ASTER) 35
Figure 18 Slope predicted thickness of regolith map (SRTM).. 35
Figure 19 Relation between thickness of regolith and elevation from ASTER (left) and SRTM DEMs (right) 36
Figure 20 Thickness of regolith and elevation with variation in slope of ASTER (a) and SRTM DEMs (b) and geology (c) and (d)... 37
Figure 21 Elevation predicted thickness of regolith map (ASTER).. 38
Figure 22 Elevation predicted thickness of regolith map (SRTM) 38
Figure 23 Predicted thickness of regolith map (ASTER)... 40
Figure 24 Predicted thickness of regolith map (SRTM) 40
Figure 25 Difference map of the predicted thickness of regolith from ASTER and SRTM DEM's......... 42
Figure 26 Site condition map based on geology and shear wave velocity 42
Figure 27 The principle of operation of GPR... 49
Figure 28 Rough terrain type GPR being used in the field. 52
Figure 29 Radar gram obtained from the field.. 52

List of tables

Table 1 Stratigraphy of the Study area 15
Table 2 Description of Statistics of elevation points 21
Table 3 Description of statistics of slope points 23
Table 4 Designation of Strength factor based on Strength of rocks. 25
Table 5 Value of shear wave velocity Vs (Ansal, 2004) 27
Table 6 Categories of soil classes based on average shear wave velocity 27
Table 7 Division of elevation classes 30
Table 8 Division of slope classes 32
Table 9 Bulk dielectric constants (measured at 100 MHz) of common earth   materials: Source (Martinez and Byrnes, 2001) 50

1. Introduction

1.1. Background

Worldwide, communities are facing an increasing frequency of a variety of disasters, among which the earthquakes are extremely hazardous. Because of their unpredictable nature, earthquakes have the potential for catastrophic loss (Stoltman et al., 2004). The effective mitigation of the seismic hazards is challenging. Ground shaking is one of the main factors that influence the damage potential of seismic hazards (Tucker et al., 1994). The thickness of regolith and its geotechnical properties characteristically modify the resultant ground shaking (Badaoui et al., 2009).

Prediction of seismic ground motion is becoming increasingly important in the mitigation of seismic hazards. Most of the theoretical models focus on large scale in isolated locations, like a single hill. Till date its application on regional scale is very limited, especially the inclusion of true surface features like thickness of regolith, topography, and local geology. These features can play a crucial role in local amplification studies. The understanding of the site response is crucial because many urban settlements where large earth quakes have happened are located on the unconsolidated deposits, like Mexico City (Mexico) in 1985, San Francisco (USA) in 1989, Los Angeles (USA) in 1995, and Ahmadabad (India) in 2001 and Muzaffarabad (Pakistan) in 2005, (Aydan, 2006; Mahajan et al., 2007).

It is therefore of crucial interest to estimate seismic amplification in such areas like Muzaffarabad and Balakot (Pakistan), before another earthquake occurs. This requires knowledge of both sub soil conditions and the possible causative seismic sources along with the availability of computational techniques that permit us to map the expected variance of ground shaking and the seismic hazard. One method of accounting for site conditions is determining the thickness of the regolith on exposed locations and linking them with geology and topographical attributes like slope and elevation to achieve a regolith thickness map. Previous studies suggests that thickness of regolith exposed in the area provide non destructive method in this regard (Devkota, 2008). Regolith can amplify earthquake ground motion causing destruction therefore, prediction of such areas of seismic variance can help in the mitigation and planning purpose (Bauer et al., 2001).

1.2. Research problem

The study area is located in northern Pakistan in one of the most seismically active regions of the world. It has witnessed major and great earthquakes in past. Recently, a major earthquake of magnitude 7.6 jolted northern Pakistan and surrounding regions, causing massive loss to human lives and economy. This was a reminder that the study area has not only suffered from earthquake devastation in past, but is also prone to major earthquakes in future (CESNED, 2006). Therefore, there is desperate need of detailed seismic hazard assessment to devise strategies to mimic the devastating effects of any future seismic activities.

The cities of the study area (Muzaffarabad and Balakot) are located on regolith, which amplifies the seismic response, intensifying the devastating effects of earthquake. Therefore estimating the spatial distribution of regolith thickness in the study area is imperative for seismic hazard zonation. The amplifying impact of regolith of seismic response has been addressed extensively, but techniques for predicting the regolith spatial variability at regional scale is being limited. This study intends to develop a numerical model predicting regolith thickness taking into consideration the topographic attributes (slope and elevation) and geology.

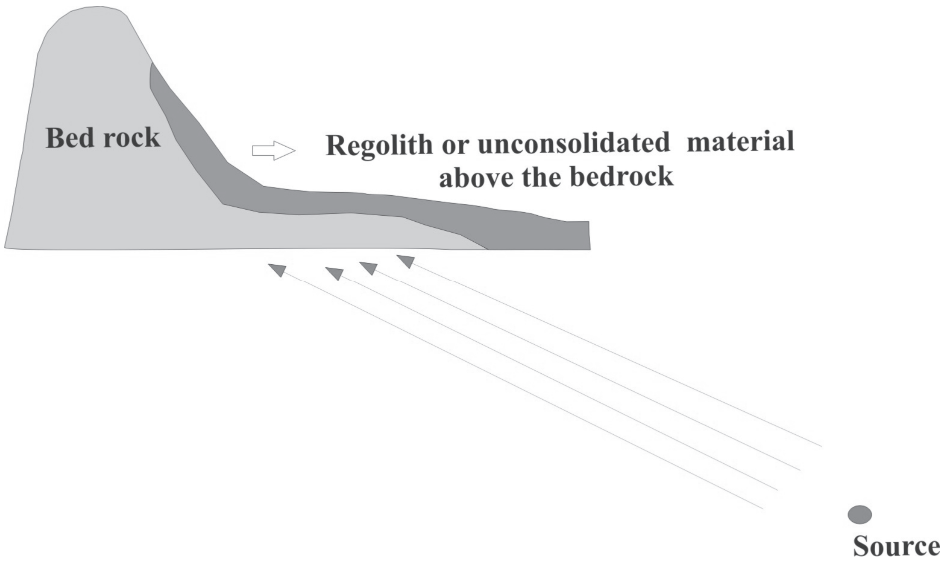

Figure 1 Variance of seismic waves due to the unconsolidated material

The boundary between bedrock and regolith as shown in the figure 1 can be marked with the help of field observation. This thickness can be related to the local conditions of geology and topography and interpolated to the regional extent to form a predicted thickness map. The prediction of the thickness of this material and its properties can help in demarcating the areas of high regional seismic amplification.

1.3. Research objective

The primary objectives of the study are:

- To predict the spatial distribution of regolith thickness by integrating field observations, geology and topographic attributes.
- To evaluate the impact of regolith thickness on seismic amplification using GIS Tools.

1.4. Sub objectives

The main objective is grouped into the following sub objectives.

- To develop the relationship of regolith thickness with geology, slope and elevation using geo-statistical tools.
- To derive a numerical model predicting spatial distribution of regolith thickness in the study area.
- To estimate the impact of thickness of regolith on seismic amplification by preparing site condition map of the study area.

1.5. Research questions

- What is the impact of geology and topographic attributes in the spatial distribution of regolith in the study area?
- Can we estimate the regolith thickness by considering geology and topographic attributes?
- What is the impact of thickness of regolith on seismic amplification in the study area?

1.6. Research hypothesis

- Local geology, slope gradient and elevation have significant influence on spatial distribution of regolith thickness.
- Shear wave velocity from literature can be utilized for estimating the seismic response of an earthquake.

1.7. Literature review

1.7.1 Factors affecting the ground seismic response

The response of a site to the incoming seismic signal plays an important role in the amplification or deamplification of the incoming signal (Yang and Yan, 2009). At a particular site, amplification due to site effects results in increased amount of ground shaking causing damage. The main factors of seismic ground shaking are source, medium and site effects as shown in figure 2.

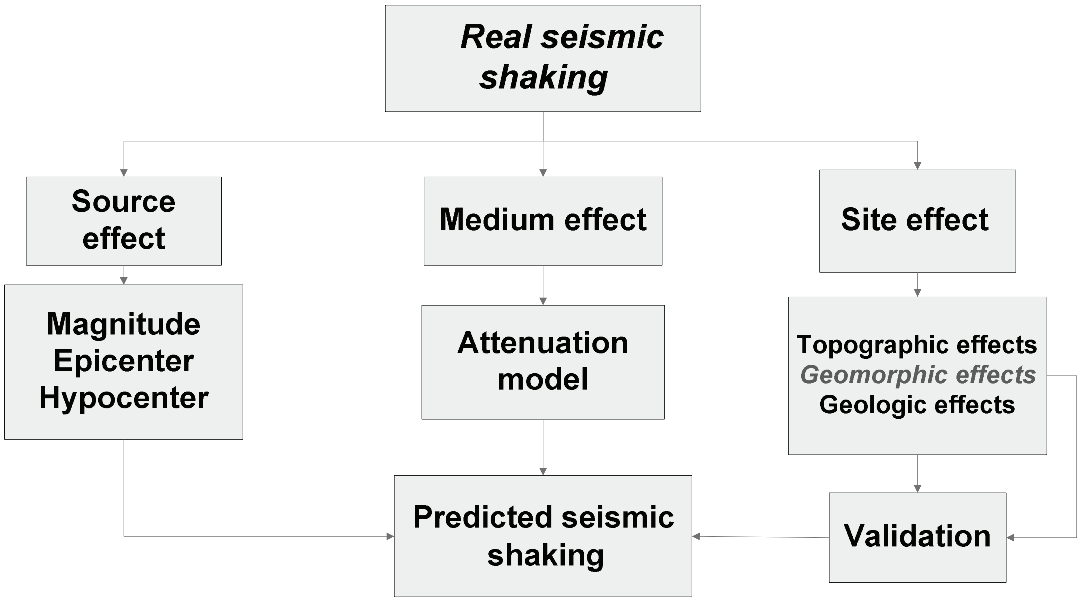

Figure 2 Framework of seismic shaking prediction, Source: (Shafique, 2008)

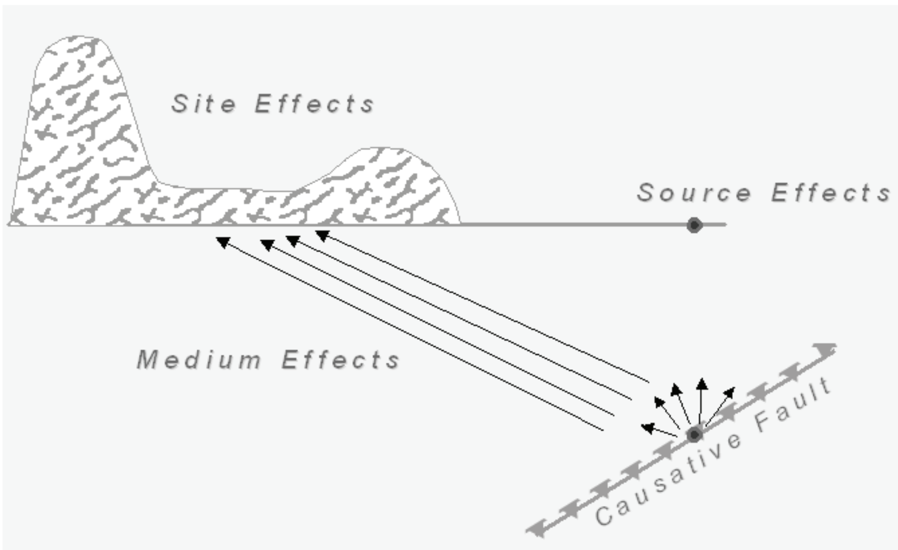

Figure 3 Factors responsible for the seismic ground shaking, Source: (Shafique et al., 2008)

Source effects are concerned with the source of the earth quake and are comprised of earthquake magnitude, epicentre, depth to hypocenter, dimensions of the rupturing fault etc (Shafique, 2008). An example of devastation caused by source and site effects is the 1999 earthquake of Kocaeli (Turkey). In this earthquake heavy damage was caused in the vicinity of the fault that was the source of earth quake ((AIJ) et al., 2001).The source parameters are calculated with the help of seismographs installed in the vicinity of the area and are publicised by the Metrological departments, United States Geological Survey (USGS), Geological Survey and certain universities. The medium of the propagation of the seismic waves alter its frequency, energy causing amplification or deamplification.

Among the site effects, local geology, topography and thickness of regolith and its geotechnical properties has significance (Rayhani et al., 2008).

1.7.2 Impact of thickness of regolith

The presence of regolith greatly affects the seismic response of earthquake e.g. the damage to the part of the bridge in Oakland which was underlain by muddy soil, in the 1989 Loma Prieta earthquake (Inglegton, 1999). Studies by (Aydan, 2006), on 2005 Kashmir earthquake highlights the presence of loose surficial and talus deposits above bedrock, intensifying the damage in Balakot as well as in Muzaffarabad. This is because of the influence of the regolith on seismic amplification that the recent geological maps discuss the quaternary deposits in detail (Wills et al., 2000). The thickness of regolith and its properties play major role in seismic response. Such as damping and impedance of the material are of prime importance from the ground shaking point of view (Pitilakis, 2004). The resistance to motion is called the impedance of a material. It depends on density, shear wave velocity of the material and the angle of incidence of the seismic waves. The higher the impedance, the higher is the stiffness of the material and thus higher the resistance to motion. Shear wave velocity of the material as an indicator of stiffness can been used for site response (Aki and Richards, 1980). It can be utilized for upper 30 m as in the general engineering practice this is a usual depth of investigations (Mahajan et al., 2007).

1.7.3 Impact of geology

Local geology can modify the characteristics of the incoming seismic waves resulting in their amplification or deamplification. Soft soil overlying bedrock almost always amplifies seismic ground shaking. Soft Recent or Quaternary deposits present at a site will respond differently than hard Cambrian igneous rocks. Geology contributes to the distribution of ground shaking and seismic induced land sliding (Kamp et al., 2008). Studies by Beauval (2003), suggests that local geology influences the duration of seismic ground motion e.g. lengthening of signal from the border to the centre of the valley.

In the seismic microzonation studies, geology of a site is crucial and is investigated thoroughly (Diego et al., 2004) . The location of faults is a basic input for the local seismic studies as they are the most likely sources of seismic energy release. They are the locations where the ground breakage and movement is expected (Jakim, 1978). In the areas that are away from the causative faults, geology plays role in the seismically triggered landsliding and liquefaction due to ground motion.

1.7.4 Impact of topography

Topography is also a factor of site effects and plays a considerable role in varying the ground shaking (Erdik and Durukal, 2004). The structures resting on the hill tops or close to steep slopes suffers more damage than those at the base due to interference of incoming seismic signal. The characteristics of amplification resulting due to topography have been studied e.g. Dhakal (2004) linked seismic amplification and slope height, fundamental frequency, wavelength and input frequency of the input signal. Studies by Shafique (2008) discusses the topographic impact on seismic amplification in the study area.

2. Study Area

The study was conducted in the area of Muzaffarabad and Balakot situated in northern areas of Pakistan and Pakistan (administered) Kashmir region as shown in the figure 4. It was severely hit by M_w 7.6 earthquake on 8th October 2005. The area and perimeter of the study site are 1265 km^2 156 Km respectively. Muzaffarabad is the capital of Pakistan administered Kashmir whereas Balakot is a city in the province of northern areas of Pakistan. Other main town in the area is Garhi Habibullah which is at a distance 40 Km from Balakot. The population density is extremely high with a value of 350 people/km^2 and the climate of the area is subtropical highland (Gazetteer, 2007).

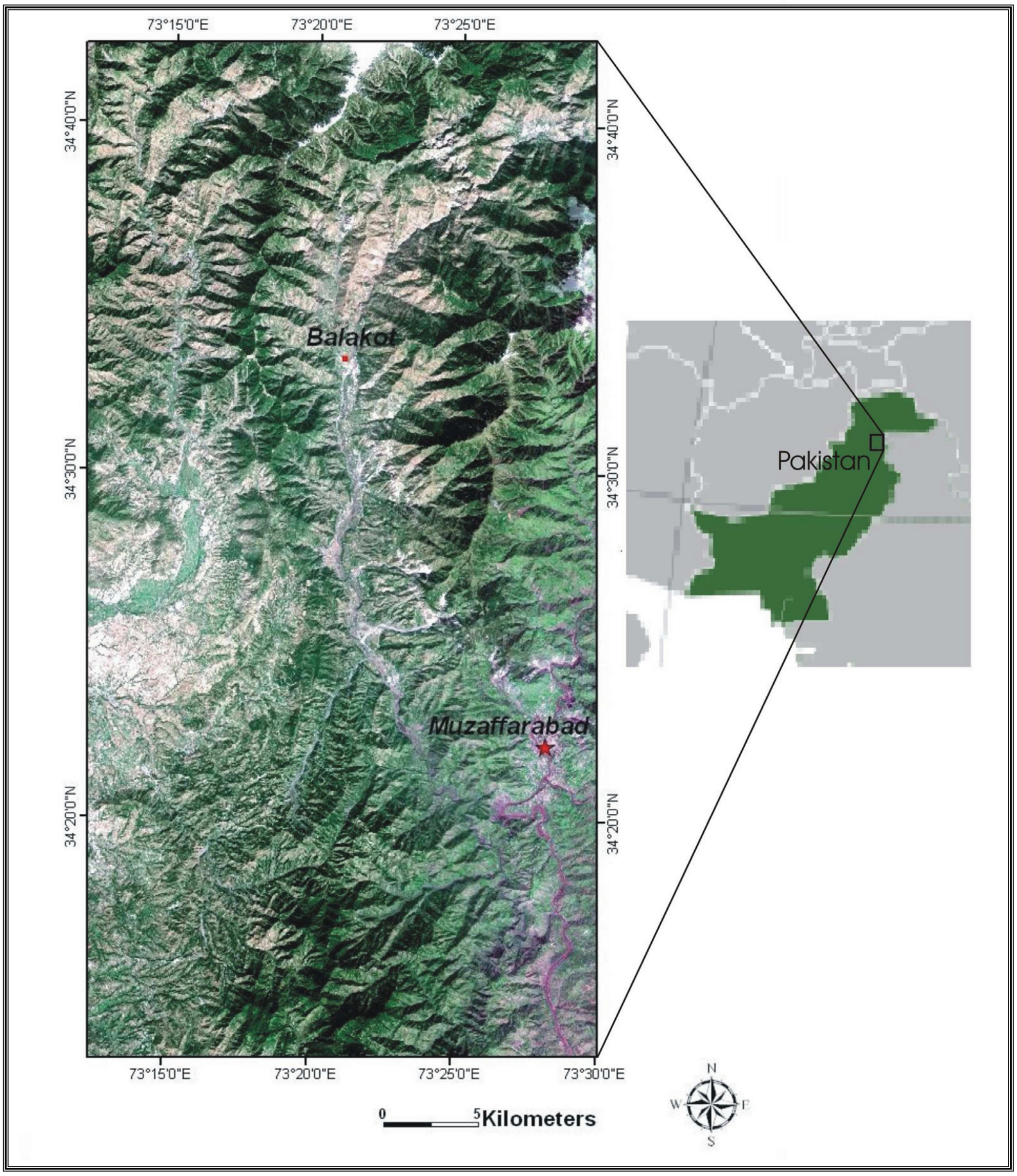

Figure 4 Location of the study area

2.1. Seismicity

The earthquakes along the Himalayan front are shown in Figure 5. In sight of the earthquakes shown in this figure, the Oct. 8, 2005 earthquake occurred in a place which can be regarded as seismic gap. However according to Aydan (2006), the gap is not fully ruptured and another earthquake having a similar magnitude may happen in the region between the location of 1842 and the 2005 earthquakes.

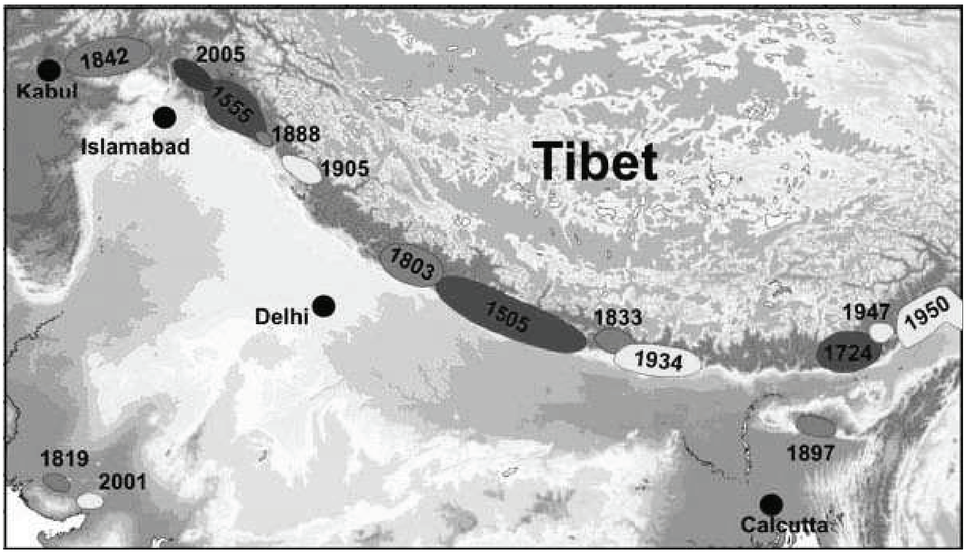

Figure 5 Large earthquakes along Himalaya region (from Wright 2005)

2.2. Geological and geomorphological setting of the study area.

The study area is mountainous. Valleys are filled by moraine and / or talus deposits originating through post glaciations and cut through by fast flowing rivers, resulting in very steep slopes (Aydan, 2006). The drainage of the area is dendritic and controlled by three main rivers Jhelum, Neelum and Kunhar with approximate discharges of 470, 240 and 80 m^3/s respectively (Pakistan Water Gateway, 2007). According to Najman et al. (2002) , the orogeny of the northern Pakistan comprises of three main tectonostratigraphic terrains i.e. the Asian plate to the north the Indian plate to the south and the Kohistan island arc sandwiched between. The study area lies in the Indian plate. As shown in the figure 7, by the geological map after (Calkins et al., 2004), the study area is covered by two geologic sheets 43 F/6 and 43 F/7 on 1:50,000 scale of Geological Survey of Pakistan. According to geological map, the study area comprises of rocks from Cambrian to Holocene, with major unconformities between, Cambrian and Jurassic, Cretaceous and Paleocene, Paleocene and Miocene and Miocene and Recent. The detailed stratigraphy of the area is given in the table 1.

Table 1 Stratigraphy of the Study area

Age	Formation / Geological Unit	Lithology
Quaternary	Terrace and stream Channel deposits.	Sand, clay, silt and gravel; loose clay and silt and gravel.
Miocene	Murree Formation	Red, purple and greenish gray shale, siltstone and conglomerate with lenses of limestone of fluvial origin.
Paleocene	Patala Formation	Dark gray shale with intercalations of marly limestone.
	Undivided	Light gray to dark gray nodular limestone and calcareous shale with intercalations of marly limestone.
	Lockhart Limestone	Light gray to dark gray nodular limestone
Late Cretaceous	Kawagarh Formation	Gray to yellowish gray, fine grained marly limestone and marl with different species of Globotruncana.
Early Cretaceous to late Jurassic	Lumshiwal and Chichali Formation	Dark gray to greenish gray and black glauconitic sandstone and shale brownish gray sandstone and limestone.
Middle Jurassic	Samana Suk Formation	Yellowish to brownish gray oolitic limestone with marly partings
Early Jurassic	Datta Formation	White sandstone and siltstone followed by red hematitic shale.
Carboniferous to Triassic	Panjal Metasediments and volcanics	Gray to greenish gray quartzite, graphitic phyllites. Green to greenish gray lava flow with tuffacous layers.
Cambrian	Abbottabad Formation	White to light gray sandstone followed by brown to gray, hard and massive medium to thick bedded cherty dolomite and limestone.
	Mansehra Orthogneiss	Augen and feldspar granite and granodioritic gneiss, megacrystic granite; intruded by tourmaline granite.
	Muzaffarabad Formation	Brown to dark gray rubbly limestone and dolomite
		Quartzite, fine grained quartzose schist with

Precambrian	Tanawal Formation	subordinate argillaceous and carbonate rocks.
	Salkhala Formation	Talc quartz mica schist, graphite schist with dolerite dikes
	Hazara Formation	Dark gray to black argillite, slate, phyllites, greywacke and siltstone, overlaid by gypsum and limestone unit.
	Manki Formation	Dark gray to black fine grained sericite bearing slate and phyllites with quartz veins.

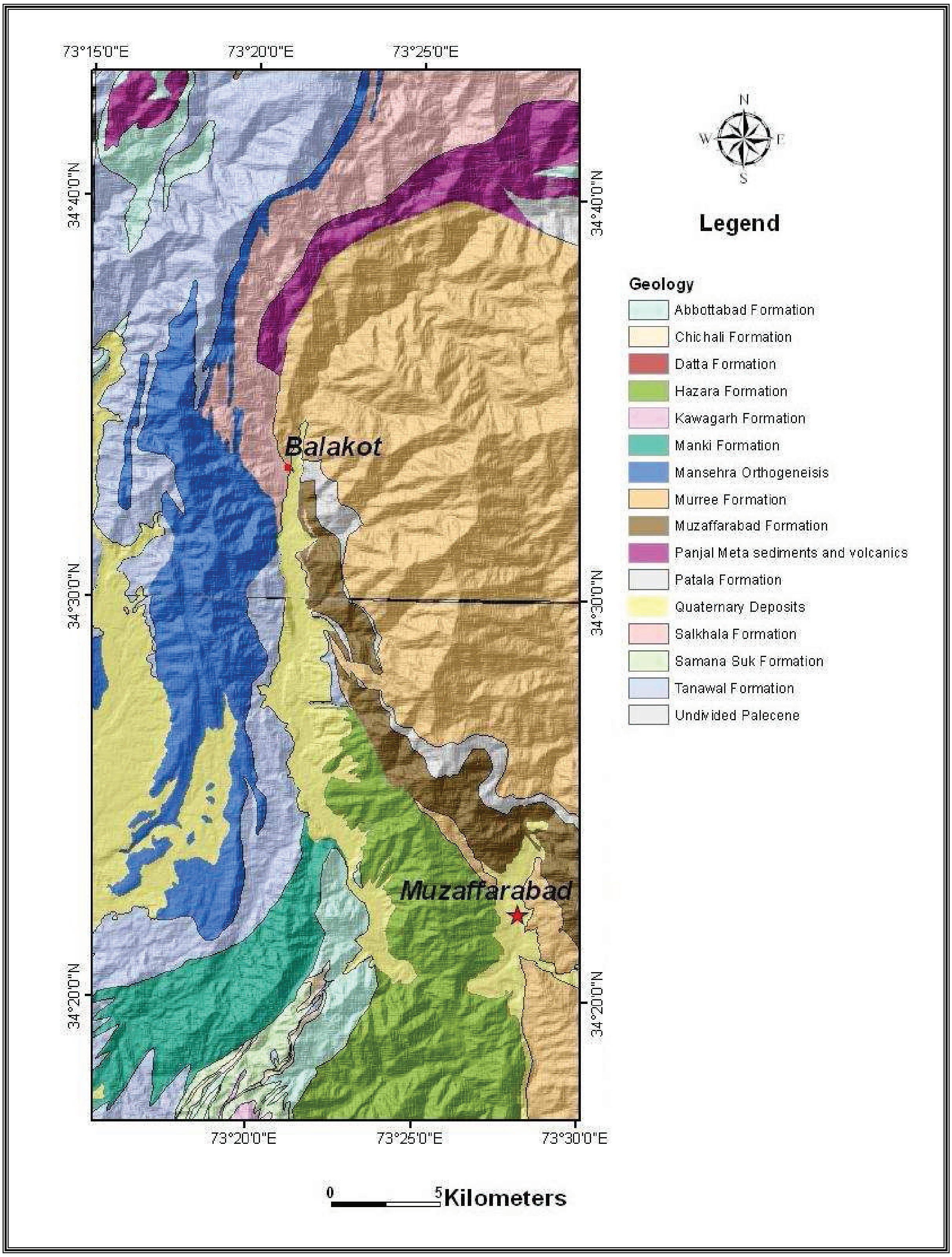

Figure 6 Geological map of the study area. Geology details in table 1. Source: (Calkins et al., 2004)

3. Material and methods

3.1. Methodology

To arrive at the objectives of the study, the research approach as shown in figure 7 was followed. The study was conceived in two parts. First the regolith thickness was determined by tape measurement taken at various localities of exposed geology, slope and elevation. GIS and geostatistical tools were utilized by deriving topographic attributes from the digital elevation models and in relating regolith thickness with the slope angle and elevation and underlying geology. The developed relation was used to prepare a predicted regolith thickness map in ArcGIS. Thus a model of regolith thickness was developed and assessed using modern statistical analysis. In the second part the impact of regolith thickness observed in the field was evaluated. This was carried out by preparing site condition map based on geology and shear wave velocity from literature which can be utilized for the assessment of seismic amplification of the site.

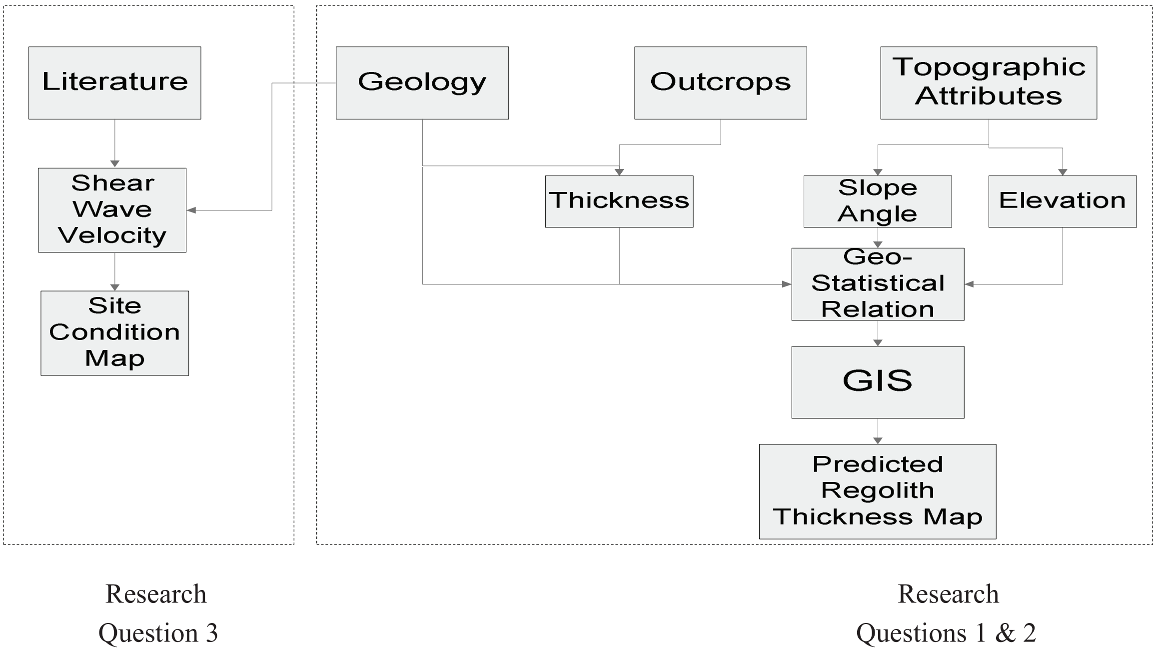

Figure 7 Flow chart of the research approach

3.2. Pre field work acitivty

The following data was available for the study.

1. Digital Elevation Models (DEM's)

• Advanced Spaceborne Thermal Emission and Reflection Radiometer (ASTER) DEM with resolution of 30m.

• Shuttle Radar Topography Mission (SRTM) DEM with resolution of 90m

2. ASTER image of November, 2005 (15m resolution).

3. Geological maps issued by the Geological Survey of Pakistan on 1:50,000 scale.

- Geological map of Balakot area (43 F/6)
- Geological map of Muzaffarabad (43 F/7)

3.3. Field data collection

Soil in the mountainous areas is formed by various soil forming processes like weathering, and organic activity and is unevenly distributed (Heimsath et al., 1999). The standard procedure for measuring regolith thickness at a constant grid can not be applied, because of the undulating topography of the study area. In the study area boundary of the regolith and bedrock was exposed along the road cuts and naturally cut slopes as shown in the figure 8. The vertical depth of the unconsolidated material above the exposed bed rock was measured with the measuring tape and is hereafter referred as the regolith outcrops. The geographic coordinates, slope, elevation and geology of these locations were also documented. The regolith outcrop observations overlaid on ASTER image are shown in the figure 9.

Figure ***8 Bedrock regolith boundary exposed in Muzaffarabad - Balakot Area***

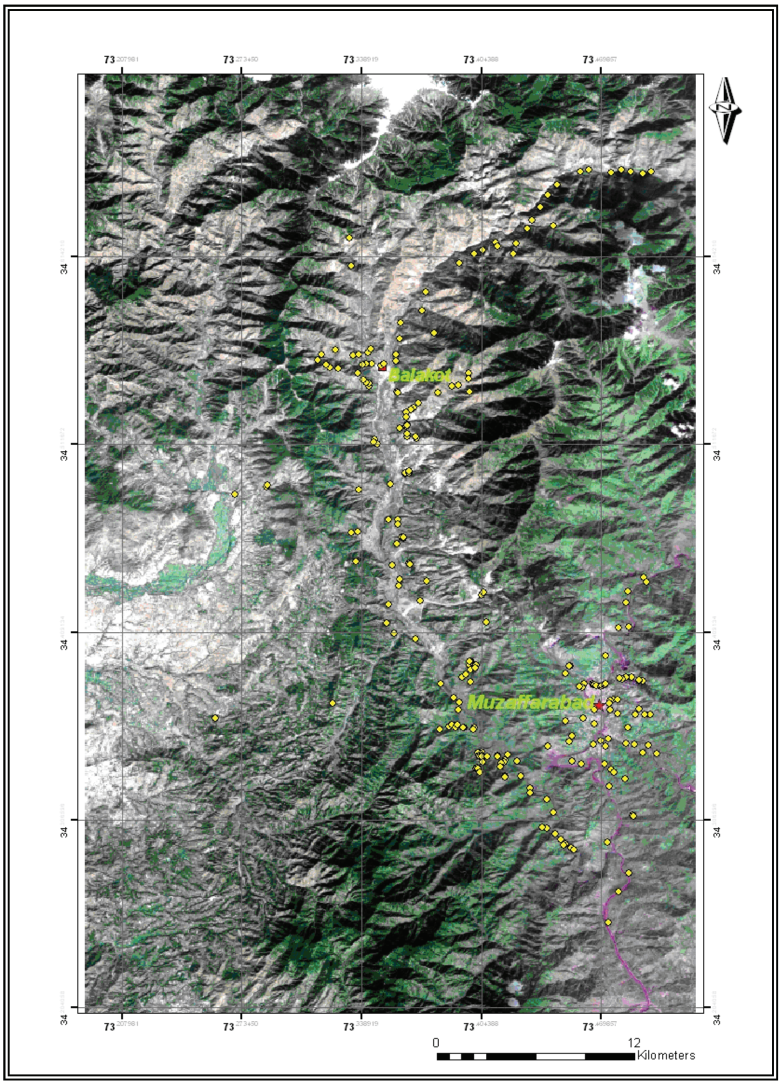

Figure 9 Regolith outcrop observations (yellow dots) over laid on ASTER image of the study area

3.4. Derivation of terrain attributes from the DEMs

As mentioned earlier ASTER and SRTM digital elevation models with different resolution were used for deriving the topographic attributes. The resolution of the digital elevation model is its ability to distinguish the size of the smallest feature. The finer the resolution the higher is the detail of information. The ASTER DEM being finer in resolution shows more details than the SRTM DEM. However elevation and slope derived from ASTER and SRTM digital elevation models may have uncertainties (Wechsler, 2006).

3.4.1. Comparison of Elevations

The outcrops were overlaid on the two digital elevation models and the elevation and slopes were extracted from them in the GIS environment. Every point on the outcrop now has three elevation and slope values i.e. from GPS or field, from ASTER and from SRTM. The table 2 shows the statistics of elevation from the ASTER and SRTM digital elevation models and GPS. The minimum and maximum values of elevation from GPS, ASTER and SRTM digital elevations model are quite close. The outcrop observations were 154.

Table 2 Description of Statistics of elevation points

S #	Source	Observations	Minimum	Maximum
1	ASTER DEM	154	623	1549
2	SRTM DEM	154	646	1556
3	GPS	154	667	1560

The elevations from the GPS were compared with those from the ASTER and SRTM digital elevation models. The Pearson correlation coefficient has been used previously for exploring the correlation between two parameters (Devkota, 2008). The correlation was found in R environment. The correlation coefficients of elevation of GPS and ASTER, GPS and SRTM and ASTER and SRTM are 0.99, 0.98 and 0.99 respectively. The scatter plots are shown in the figure 10. With this comparison we can say that in this study the elevation extracted from elevation of GPS and ASTER, GPS and SRTM and ASTER and SRTM digital elevation models are highly correlated.

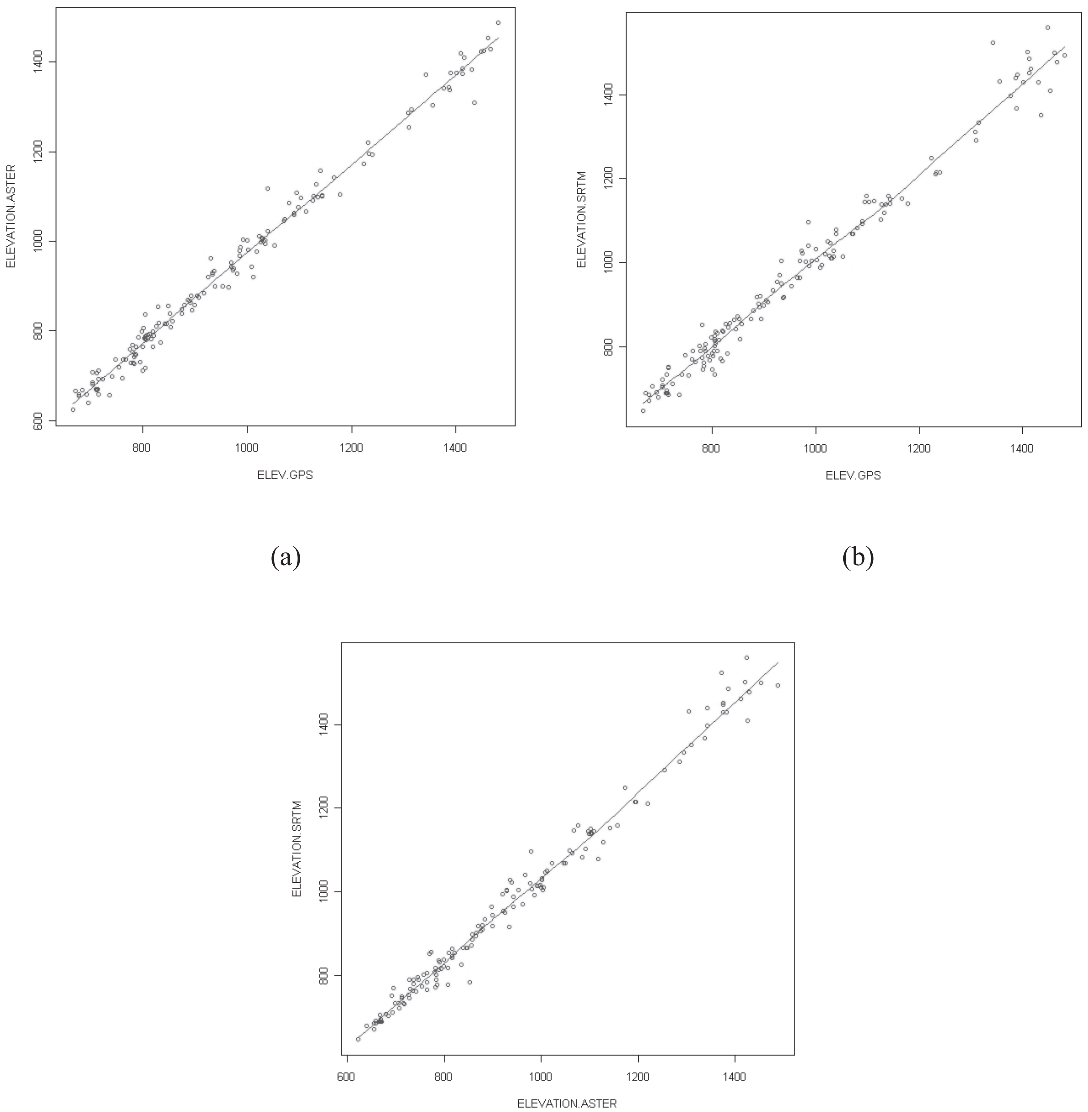

(a) (b)

(c)

Figure 10 Correlations of GPS elevation and ASTER (a), GPS and SRTM DEM (b) and between ASTER and SRTM DEMs (c)

3.4.2. Comparison of slopes

The slopes derived from ASTER and SRTM digital elevation models were also compared with those from field observations. The maximum and minimum slope (degrees) values are given in the table 3; the minimum values of slope from field, ASTER and SRTM digital elevations model are closer than the maximum values. The correlation coefficient of slopes of field and SRTM, field and ASTER and ASTER and SRTM are 0.25, 0.20 and 0.15 respectively. The scatter plots are shown in the figure 11 this comparison implies that in our study although the slope extracted from ASTER and SRTM digital elevation models are slightly correlated to the slopes from field. However slope extracted from ASTER and SRTM digital elevation models are not much related.

Table 3 Description of statistics of slope points

S #	Source	Observations	Minimum	Maximum
1	Aster DEM	154	1.6	61.25
2	SRTM DEM	154	2.19	45.08
3	Field	154	0	90

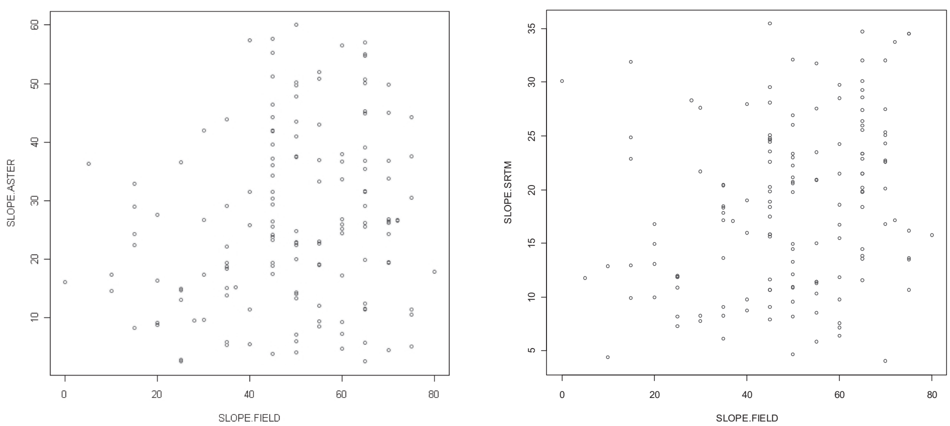

(a) (b)

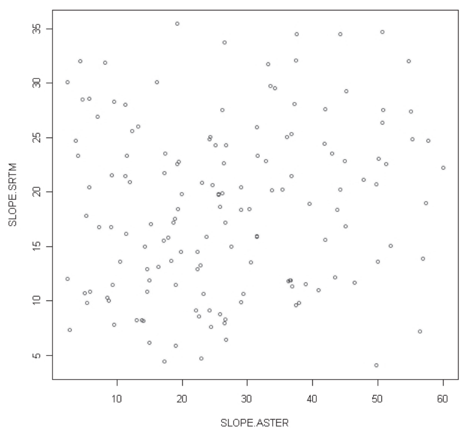

(c)

Figure 11 Correlations of slopes derived from field and ASTER (a), field and SRTM DEM (b) and ASTER and SRTM DEMs (c)

3.4.2. Modelling thickness of regolith

The field measurements were carefully checked before carrying out the analysis. Based on the field measurements a geostatistical relationship was developed between thickness of regolith and slope, elevation and geology. Previously soil properties have been modelled by using comprehensive statistical tool for data analysis like Sapkota (2008).

In this study the correlations between thickness of regolith and slope, elevation and geology were visualized using scatter plots and comparing Pearson correlation coefficients. A linear regression analysis was used to develop relations of thickness of regolith with each surface feature. Thickness of regolith was considered as response and slope, elevation and geology as explanatory variables. The relation thus developed was used to form a predicted map for each feature. Finally a multiple linear regression analysis was applied according to the collected data. Multiple linear regression relates a response or dependant variable and explanatory or independent variable by applying an equation of straight line to the data (Field, 2005). The general relation is given as follows.

$$\mathbf{Y = (b_o + b_1X_1 + b_2\,X_2 + b_3\,X_3 \ldots\ldots\ldots b_nX_n) + \varepsilon_i \ldots\ldots\ldots\ldots\ldots\ldots\ldots Equation\ 1}$$

Where

Y = Response variable

b_o = Y-intercept (X=0)

b_1 = Coefficient of the first predictor $X_{1,}$

b_2 = Coefficient of the second predictor X_2

b_3 = Coefficient of the third predictor X3

b_n = Coefficient of the nth predictor X_n ,

ε_i = Difference between the predicted and observed value of Y for the i^{th} participant.

Based on this relation an integrated map was prepared. As the slope and elevation were derived from ASTER and SRTM digital elevation models two relations and hence two predicted thickness of regolith maps were produced. The geological units were assigned numerical values (strength factors) according to the strength of the rocks from 0.25 to 1 as shown in the table 4. Soft rocks like Quaternary deposits were assigned a value of 1 and the hard rocks like quartzite, granites and hard Precambrian and Cambrian dolomite and limestone were assigned 0.25. Like this Paleocene to Miocene sedimentary rocks were designated as medium soft and assigned strength factor of 0.75 along with Precambrian slate and schists and fractured Cambrian rocks. Carboniferous to Late Cretaceous lithologies were designated as medium hard with a strength factor of 0.5. After running the regression model based on these values of geology, slope and elevation a geostatistical relation was developed in R environment. The coefficient and the significance of the model were discussed. Finally this relation was used to form a regolith thickness map in ArcGIS.

Table 4 Designation of Strength factor based on Strength of rocks.

Age	Formation/ Geological Unit	Lithology	Strength Factor
Quaternary	Terrace and stream Channel deposits.	Sand, clay, silt and gravel; loose clay, silt and gravel.	1
Miocene	Murree Formation	Red, purple and greenish gray shale, siltstone and conglomerate with lenses of limestone of fluvial origin.	0.75
Paleocene	Patala Formation	Dark gray shale with intercalations of marly limestone.	0.75
	Undivided	Light gray to dark gray nodular limestone and calcareous shale with intercalations of marly limestone.	0.75
	Lockhart Limestone	Light gray to dark gray nodular limestone	0.75
Late Cretaceous	Kawagarh Formation	Gray to yellowish gray, fine grained marly limestone and marl with different species of Globotruncana.	0.5
Early Cretaceous to late Jurassic	Lumshiwal and Chichali Formation	Dark gray to greenish gray and black glauconitic sandstone and shale brownish gray sandstone and limestone.	0.5
Middle Jurassic	Samana Suk Formation	Yellowish to brownish gray oolitic limestone with marly partings	0.5
Early Jurassic	Datta Formation	White sandstone and siltstone followed by red hematitic shale.	0.5
Carboniferous to Triassic	Panjal Metasediments	Gray to greenish gray quartzite, graphitic phyllites. Green to greenish gray lava flow	0.5

	and volcanics	with tuffacous layers.	
Cambrian	Abbottabad Formation	White to light gray sandstone followed by brown to gray, hard and massive cherty dolomite and limestone.	0.25
	Mansehra Orthogneiss	Augen and feldspar granite and granodioritic gneiss, megacrystic granite; intruded by tourmaline granite.	0.25
Precambrian	Muzaffarabad Formation	Brown to dark gray rubbly limestone and dolomite	0.50
	Tanawal Formation	Quartzite, fine grained quartzose schist with subordinate argillaceous and carbonate rocks.	0.25
	Salkhala Formation	Talc quartz mica schist, graphite schist with dolerite dikes	0.75
	Hazara Formation	Dark gray to black argillite, slate, phyllites, greywacke and siltstone, overlaid by gypsum and limestone unit.	0.75
	Manki Formation	Dark gray to black fine grained sericite bearing slate and phyllites with quartz veins.	0.75

3.5. Construction of site condition map

The consideration of geotechnical properties of the underlying material is important for any site characterization for seismic amplification (Srbulov, 2009). The engineering properties like shear wave velocity has long been accredited as a contributing factor in ground motion amplification and site response (Borcherdt, 1970; Mahajan, In Press). Studies suggests that it is an indicator of stiffness of the material present beneath a site (Aki and Richards, 1980; Bullen, 1963; Mahajan et al., 2007). To consider the seismic condition of site, a site condition map based on geology and shear wave velocity can be constructed (Wills et al., 2000). The shear wave velocity values according to the strength of the rocks can be assigned to the site as described in the table 5.

Table 5 Value of shear wave velocity Vs *(Ansal, 2004)*

Soil Class	Description	Properties
A	Hard rock	V_s > 1500 m/Sec
B	Rock	760 m/Sec < V_s < 1500 m/Sec
C	Very dense soil and soft rock	360 m/Sec < V_s < 760 m/Sec
D	Stiff soil	180 m/Sec < V_s < 360 m/Sec
E	soil	V_s < 180 m/Sec

A site condition map for the study area was constructed. The methodology followed resembles that used by Peterson et al (1997), who categorized the geological units according to strength from hard to soft. The map was digitized and generalized from 1:50,000 geological maps (figure 6) and the shear wave velocities were assigned to the formations based on strength of the rocks according to table 1. The geological formations in the study area range in age from Precambrian to Recent. The shear wave velocity values were assigned based on the dominant lithology present in the rock unit (table 1). For example the dominant lithology in Hazara formation was slate so it was assigned a category of "C" in the soil class, Tanawal formation mainly comprised of quartzite therefore it was categorized as "A" in the soil class. Table 6 shows the categories of the soil classes and the assigned average shear wave velocity of each class present in the study area. The soil class "D" and "E" were merged as "D" for simplicity.

Table 6 Categories of soil classes based on average shear wave velocity

Description	Soil Class	Average shear wave velocity
Hard rock	A	1500
Rock	B	1130
Very dense soil and soft rock	C	560
Soil	D	180

4. Results and discussions

The thickness of regolith measured in the field was related to the underlying geology and topographic attributes slope and elevation using the method described in the section 3.4.3. Previous studies have shown that surface features have an effect both on the thickness of regolith (Devkota, 2008) and the seismic amplification. GIS and statistical methods based on spatial data has been used previously such as Remondo et al. (2003).

4.4. Relationships between thickness of regolith and geology.

The geology of the site can be associated to the thickness of regolith. Thickness is higher in the areas underlain by the lithologies that are non-resistant to weathering (Anand and Paine, 2002). Figure 12 shows the relation between geology and regolith thickness. The highest thickness of 10 m is observed in the Quaternary rocks and minimum of 2m in the Precambrian and Cambrian hard rocks. The Pearson correlation coefficient is 0.36, which indicates the relation of geology and thickness of regolith.

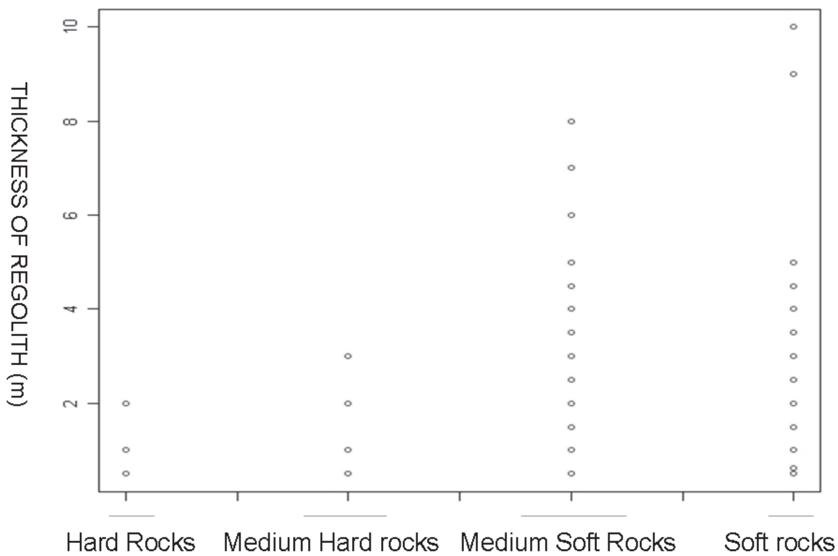

Figure 12 Correlation between Geology and thickness

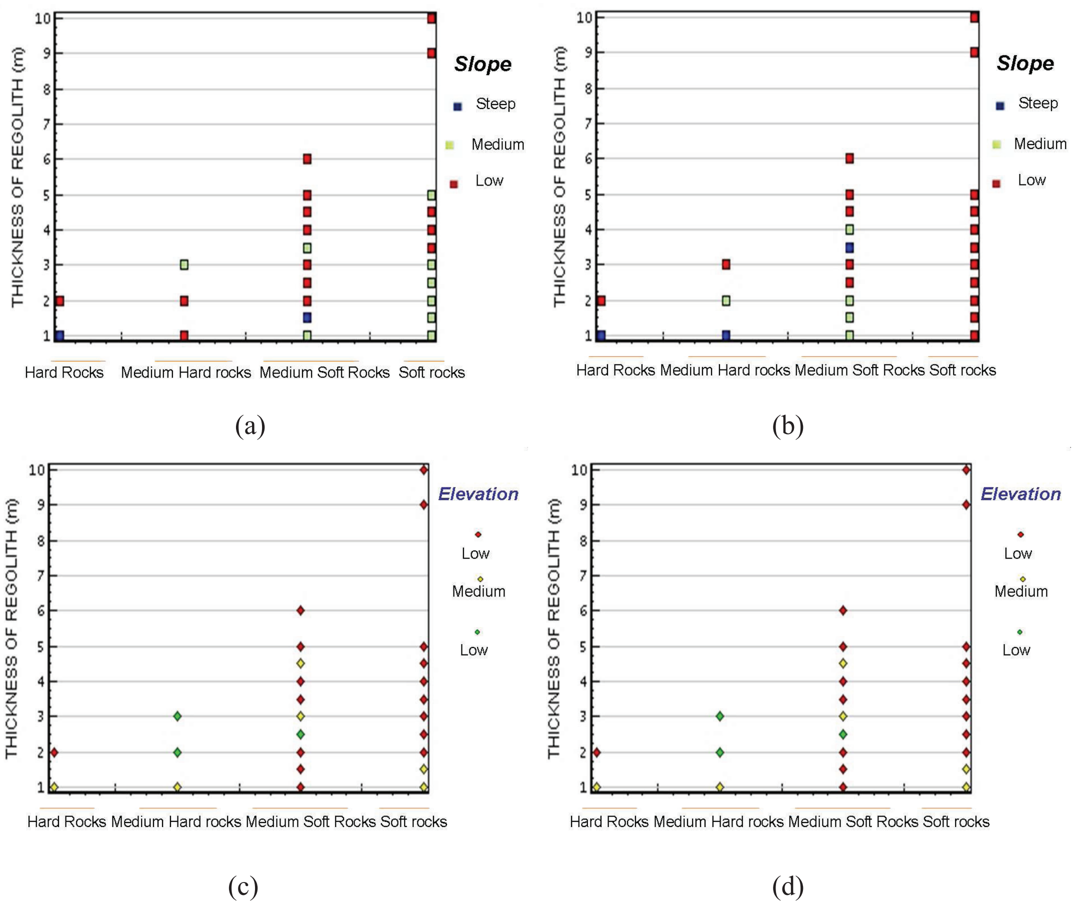

Figure 13 Thickness and geology with variation in slope and elevation of ASTER (a) and (c) and SRTM (b) and (d) respectively

The figure 13 (a and b) shows the relation between thickness of regolith and geology with variation in slopes of ASTER and SRTM digital elevation models respectively. It illustrates that the thickness is higher where the soft rocks are present at lower or flatter slopes and less where hard rocks are exposed with steeper slopes. Some low sloping soft rocks have less thickness because the measurements were taken along the road sides where erosion has taken place.

The relation between thickness of regolith and geology with variation in elevation of ASTER and SRTM digital elevation models is illustrated in the figure 13 (c and d) respectively. Thickness of the regolith is more where the soft rocks are exposed on lower elevations and less where hard rocks are present at higher elevations. The division of elevation classes is given in the table 7. The elevations derived from ASTER and SRTM digital elevation models were classified with the same divisions. The elevations derived from ASTER and SRTM digital elevation models were highly correlated therefore scatter plots in figure 13 (c) and (d) are the same.

Table 7 Division of elevation classes

Elevation Class	Low	Medium	High
ASTER Elevation (m)	623 - 919	919 - 1214	1214-1549
SRTM Elevation (m)	646 - 919	919 - 1214	1214-1556

The linear relation of geology with thickness of regolith as described in the section 3.4.2. is given in the equation 2.

$$\textbf{Thickness of regolith} = \mathbf{3.30 \times Geology - 0.13} \qquad \textbf{Equation 2}$$

The p-value of the relation is 0.0005 which reveals that it is highly significant. Based on this relation geology predicted thickness of regolith map as shown in the figure 14 was prepared.

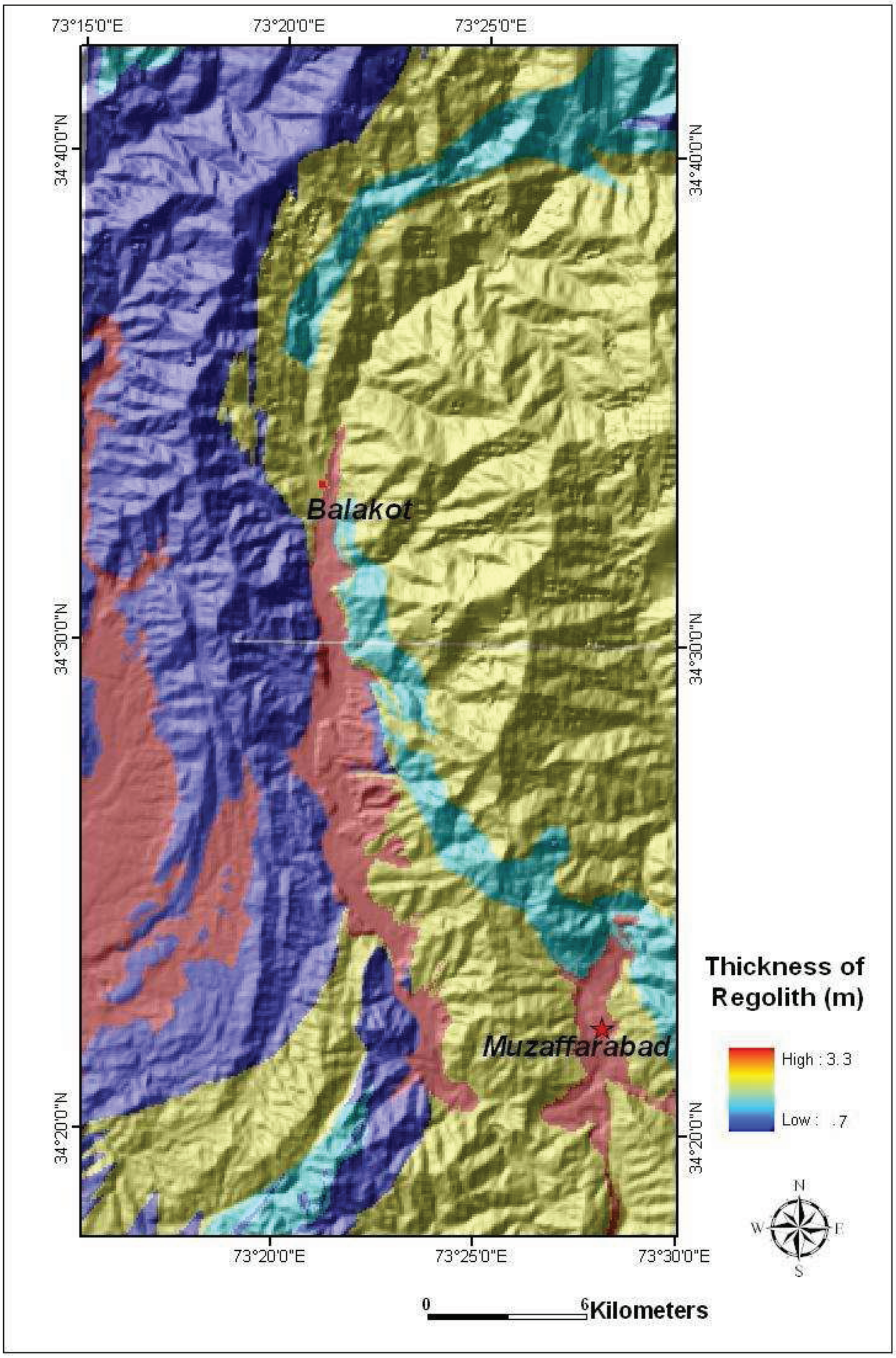

Figure 14 Geology predicted thickness of regolith map

This map shows the distribution of regolith based on geology. The predicted thickness of regolith ranges from 3.3 to 0.7m. It is higher in the centre of the valleys and on the exposures where soft and medium soft rocks such as quaternary deposits, slates, schists and shale, exhibits more thickness whereas hard rocks like quartzite and granitic rocks show less cover of regolith.

4.5. Relationships between regolith thickness and topographic attributes.

An attempt was made to relate regolith thickness with elevation and slope derived from SRTM and ASTER digital elevation models. The derived slope values are given in the table 8. These values were classified for visualization in scatter plots as given by the table below.

Table 8 Division of slope classes

Slope Class / DEM	Low	Medium	Steep
ASTER	0-20	20-40	40-65
SRTM	0-18	18-26	26-45.08

4.5.2. Relationships of thickness of the unconsolidated material and slope

The relation of thickness of regolith decreases and slope of ASTER and SRTM digital elevation models are shown in the figure 15. The thickness of regolith and slope are inversely related to each other. The thickness of regolith decreases with the increases in slope and increases with the decrease in slope. Studies by (Ellenkamp, 2004) also found the same relation. The Pearson correlation coefficients of thickness of regolith and slopes of ASTER and SRTM digital elevation models are -0.42 and -0.48 respectively.

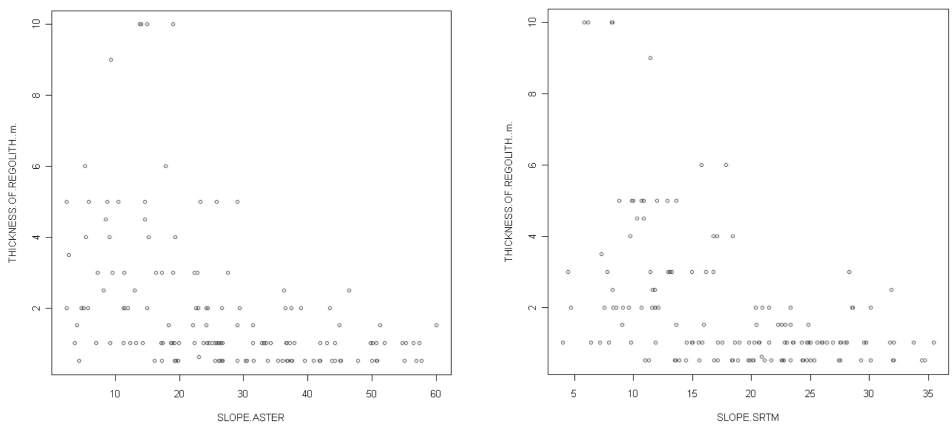

Figure 15 Correlation between thickness of regolith and slope of ASTER (left) and SRTM DEMs (right)

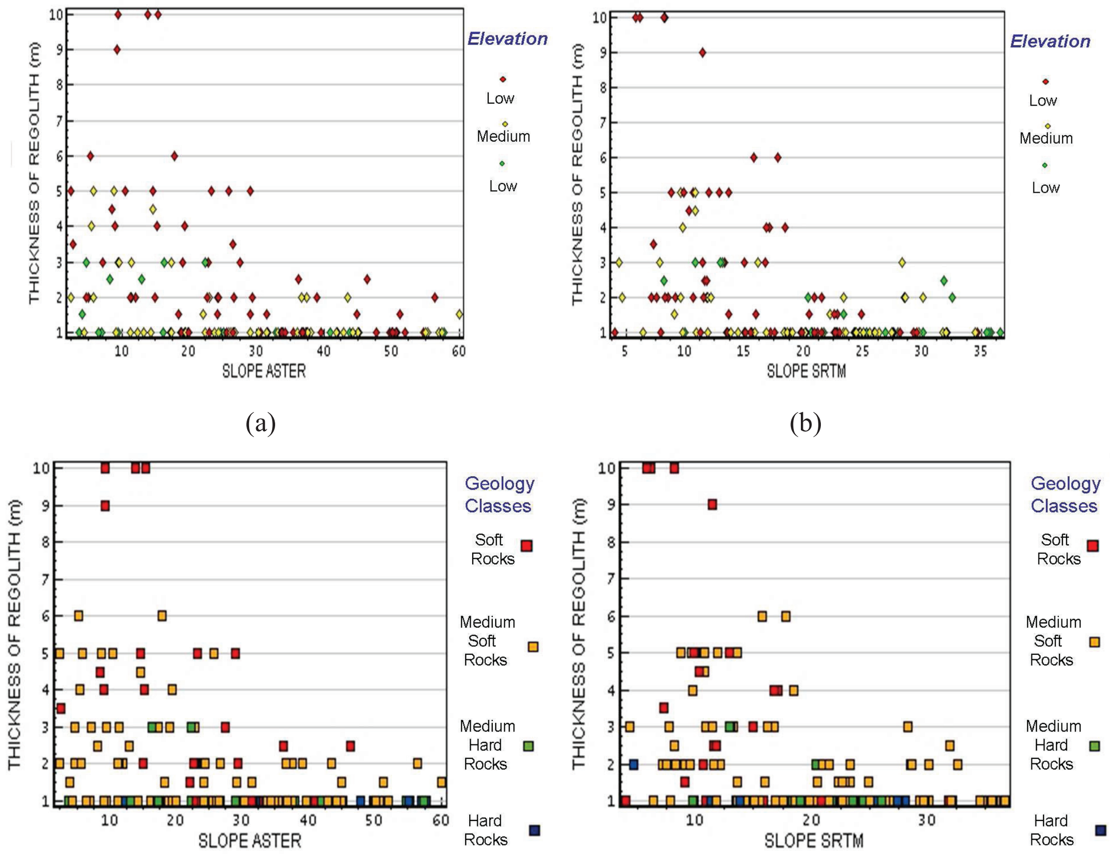

(a) (b)

(c) (d)

Figure 16 Thickness of regolith and slope with variation in elevation of ASTER (a) and SRTM DEMs (b) and geology (c) and (d)

The thickness of regolith and slopes of both digital elevation models were analysed by variation of elevation for both digital elevation models and geology. Figure 16 graphically represents the relation between thickness and slope with variation in elevation of ASTER (a) and SRTM (b). The thickness is higher where there is a combination of low slopes and low elevation and less where steep slopes are found in the higher elevations.

The relation of thickness of regolith and slope with variation of geology is shown graphically in the figure 16 (c) and (d) for the slope derived from ASTER and SRTM digital elevation models. Thickness of regolith is more when there is a combination of soft rocks and low slope and less when hard rocks are exposed with steeper slopes.

The linear relations of thickness of regolith and slopes of ASTER and SRTM digital elevation models are given in the equations 3 and 4 respectively.

$$\textbf{Thickness of regolith} = 3.4 - 0.063 \times \textbf{Slope} \qquad \textbf{Equation 3}$$

The p-value of the relation is $9.31e^{-08}$ which reveals that it is highly significant.

$$\textbf{Thickness of regolith} = 4.0 - 0.09 \times \textbf{Slope} \qquad \textbf{Equation 4}$$

The p-value of the relation is $4.9e^{-05}$ which reveals that it is highly significant. The prediction of regolith thickness maps based on these relations are shown in the figures 17 and 18 respectively. The thickness of regolith is higher in the low sloping areas and less in the steeper areas. The maximum thickness of regolith predicted from slopes of ASTER and SRTM digital elevations models are 3.4 and 4m. This difference can be attributed to the low correlation of slope in this study which is shown by the Pearson correlation coefficient of 0.15 between slopes of ASTER and SRTM digital elevations models (figure 11).

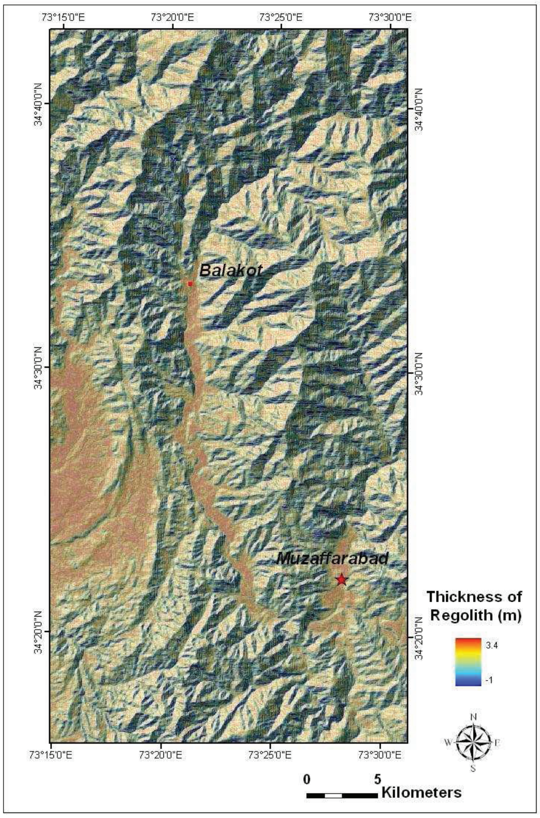

Figure 17 Slope predicted thickness of regolith map (ASTER)

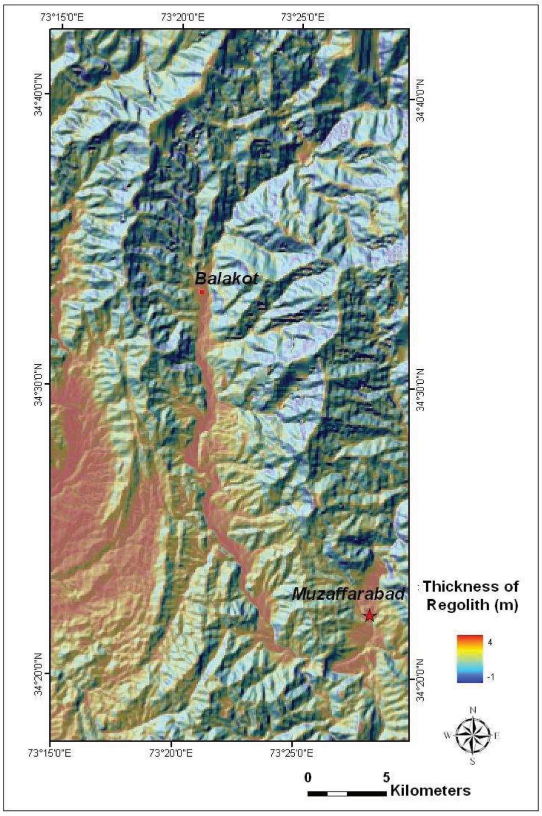

Figure 18 Slope predicted thickness of regolith map (SRTM)

4.5.3. Relationships of thickness of the unconsolidated material and elevation

There is an inverse relation between thickness of regolith and elevation. Thickness of regolith decreases with the increases in the elevation of both ASTER and SRTM digital elevation models as shown in the figure 19. However, this relation is specific for the area of study; other higher areas may have more thickness depending upon the surface features. The Pearson correlation coefficient of thickness of the unconsolidated material and elevation derived from the ASTER and SRTM digital elevation models is -0.28 and -0.27 respectively as shown by the scatter plots in the figure 19.

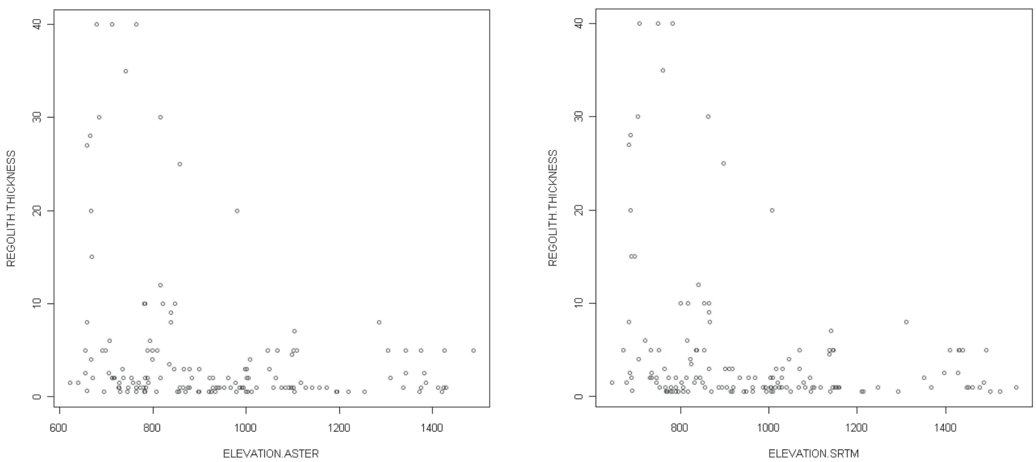

Figure 19 Relation between thickness of regolith and elevation from ASTER (left) and SRTM DEMs (right)

The thickness of regolith and elevation derived from ASTER and SRTM digital elevation models were analysed by variation of slopes and geology. Figure 20 represents the relation between thickness and elevation with variation in slope ASTER (a) and SRTM (b). The thickness is higher when there is a combination of low slopes and low elevation and less where steep slopes are found in the higher elevations.

The relation of thickness of regolith and elevation with variation of geology is shown graphically in the figure16 (c) and (d). Thickness of the regolith is more when there is a combination of soft rocks and low elevation and less when the hard rocks are exposed with higher elevation.

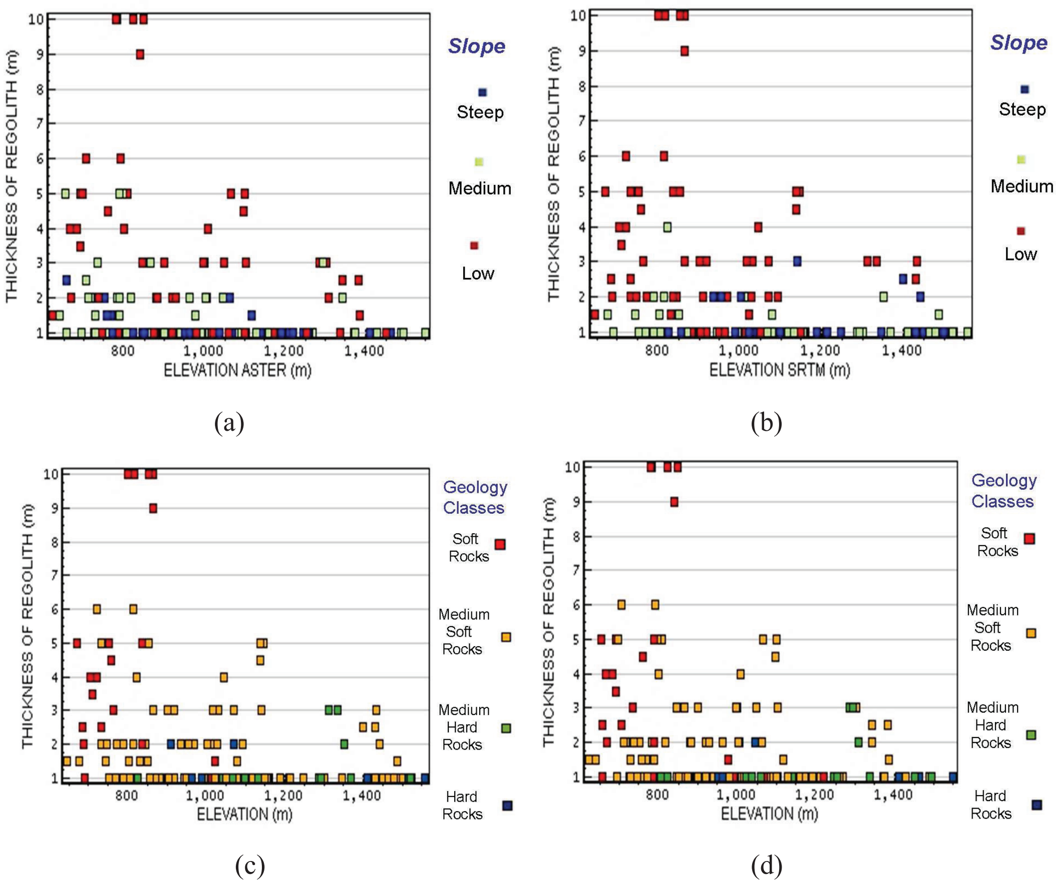

Figure 20 Thickness of regolith and elevation with variation in slope of ASTER (a) and SRTM DEMs (b) and geology (c) and (d)

The relations of thickness of regolith and elevations of ASTER and SRTM digital elevation models are given in the equations 5 and 6 respectively. The prediction of regolith thickness maps based on these relations are shown in the figures 21 and 22 respectively.

Thickness of regolith = 3.41 – 0.0012×Elevation **Equation 5**

Thickness of regolith = 3.36 – 0.0011×Elevation **Equation 6**

The significance of the relations of regolith thickness with elevations of ASTER and SRTM digital elevation models are 0.14 and 0.16 respectively according to the p-value of the relation,the significance is less as compared to that of slope and geology.

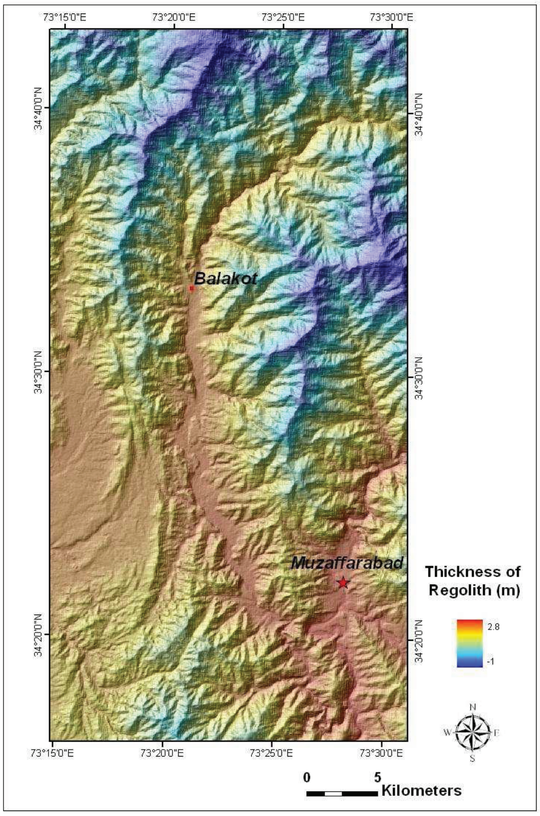

Figure 21 Elevation predicted thickness of regolith map (ASTER)

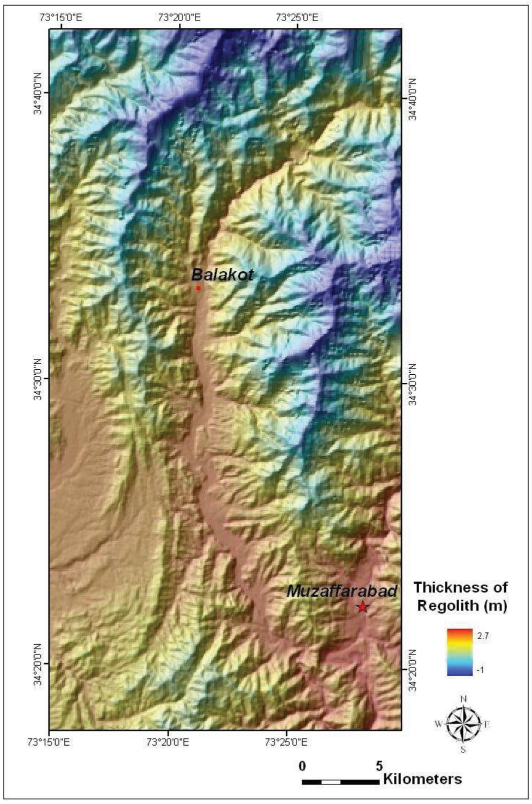

Figure 22 Elevation predicted thickness of regolith map (SRTM)

The thickness of regolith is higher in the low elevation areas and less in the high elevation areas. The maximum thickness of regolith predicted from elevation of ASTER and SRTM digital elevations models are 2.8 and 2.7m respectively. This can be attributed to the high correlation shown by the Pearson correlation coefficient of 0.99 between elevations of ASTER and SRTM digital elevations models (figure 10).

4.6. Maps of thickness of regolith

Based on the field observations, thickness of regolith was related to slope, elevation and geology from both ASTER and SRTM digital elevations models. The relations for both ASTER and SRTM digital elevation models are given in the equations 7 and 8 respectively. The predicted thickness of regolith maps based on these equations are shown in the figures 23 and 24.

Thickness of regolith = 2.73 + 2.21 $\times$ geology – 0.05 $\times$ Slope – 0.0005 $\times$ Elevation **Equation 7**

The adjusted R-square and p-value of the relation are 0.20 and $5.7e^{-08}$ respectively. P-value (<0.05) reveals that it is highly significant however the adjusted R-square indicates that the model explains the 20 % of total variance of the regolith thickness. The coefficients of slope geology and elevation reveal the sensitivity of the model i.e. if one variable is held constant what will be its effect on regolith thickness. If slope and elevation are held constant then each unit rise in the geology class will increase regolith thickness by 2.21m. It is important to note here that four geology classes have been used. If geology and elevation are held constant then each unit rise in the slope will increase regolith thickness by 0.05m. Similarly if geology and slope are held constant then each unit rise in the elevation will increase regolith thickness by 0.0005m.

Thickness of regolith = 1.03 + 2.81 $\times$ geology – 0.08 $\times$ Slope – 0.0008 $\times$ Elevation **Equation 8**

The adjusted R-square and p-value of the relation are 0.14 and $1.6e^{-05}$ respectively. P-value reveals that it is highly significant however the adjusted R-square indicates that the model explains the 14 % of total variance of the regolith thickness. If slope and elevation are held constant then each unit rise in the geology class will increase regolith thickness by 1.03m. If geology and elevation are held constant then each unit rise in the slope will increase regolith thickness by 0.08m. Similarly if geology and slope are held constant then each unit rise in the elevation will increase regolith thickness by 0.0008m. The adjusted R-square and p-values of models derived from ASTER and SRTM digital elevation models can be utilized for comparison. The model derived from ASTER digital elevation model explains more variation and the p-values are more significant than that of SRTM digital elevation model.

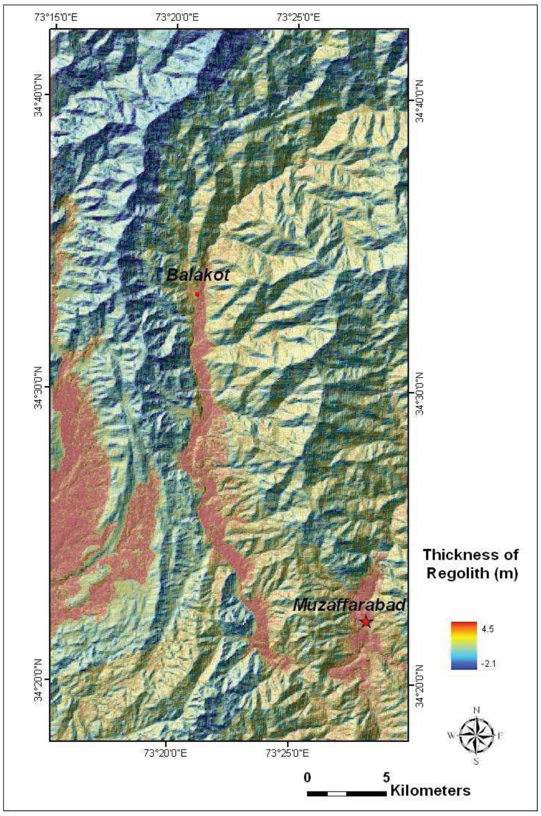

Figure 23 Predicted thickness of regolith map (ASTER)

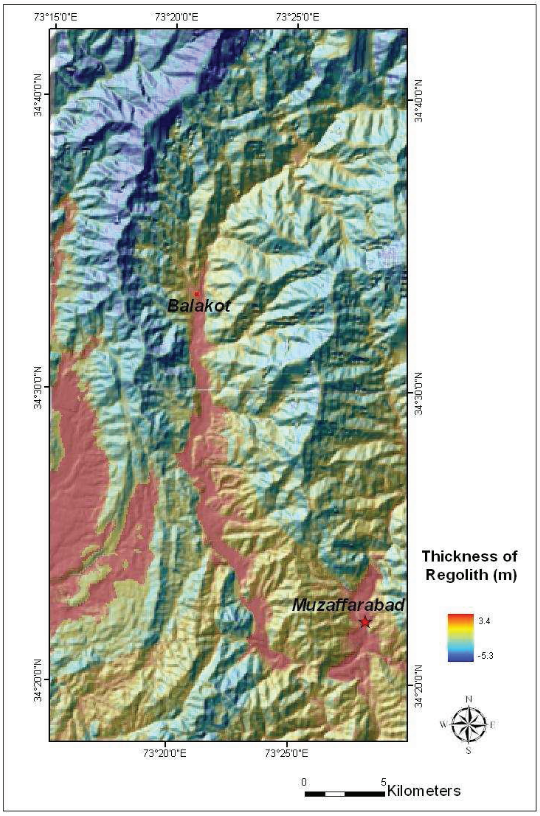

Figure 24 Predicted thickness of regolith map (SRTM)

The maximum predicted thickness of regolith from ASTER and SRTM digital elevations models are 4.5 and 3.4m respectively. The negative value is assumed to have no thickness of regolith due to erosion. The thickness of regolith is more in the areas with low slope and elevation underlain by soft rocks. Moreover at steep slopes, high elevation and hard rocks beneath the site thickness of regolith is less to absent. A map showing the difference of the models from ASTER and SRTM digital elevations models is shown in the figure 25. This map shows that there is more difference of regolith thickness predicted in the areas with steep slopes and higher altitude. However in the centre of the valleys the difference is less.

4.7. Site condition map

The site condition map based on categories of geology and shear wave velocity is shown in the figure 26. This map provides an initial estimate of stiffness of surficial material that can solely be used or with other factors in calculating seismic hazards. The value of shear wave velocity as a gauge of stiffness ranges from 180 to 1500 MHz. The map shows the spatial distribution of stiffness of the material present in the area. The low stiff material is present in the valleys. It is important to note that both Balakot and Muzaffarabad cities are located on same class D that have low shear wave velocity material. This map can also be utilized for calculating natural time period of the site using the equations 9 (Kim et al., 2002) respectively. However this map can be improved by inclusion of observed values of V_s and using a larger scale of geological map.

$$\mathbf{T_o = 4H / V_s} \qquad \textbf{Equation 9}$$

Where T_o is the natural time period site, H is the regolith thickness and V_s is the shear wave velocity.

4.8. Chapter of ground penetrating radar

Application of ground penetrating radar GPR) to determine the regolith thickness in the study area was not concluded. This chapter is included as “Results of ground penetrating radar” in appendix 1.

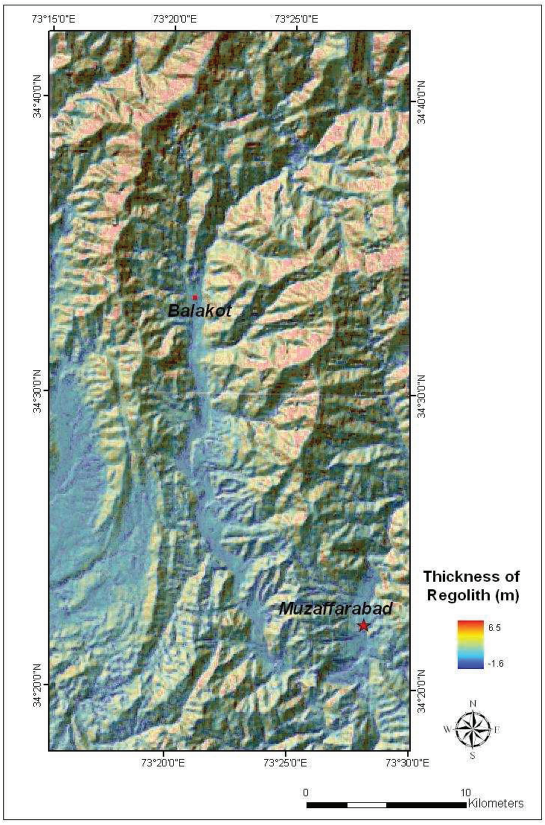

Figure 25 Difference map of the predicted thickness of regolith from ASTER and SRTM DEM's

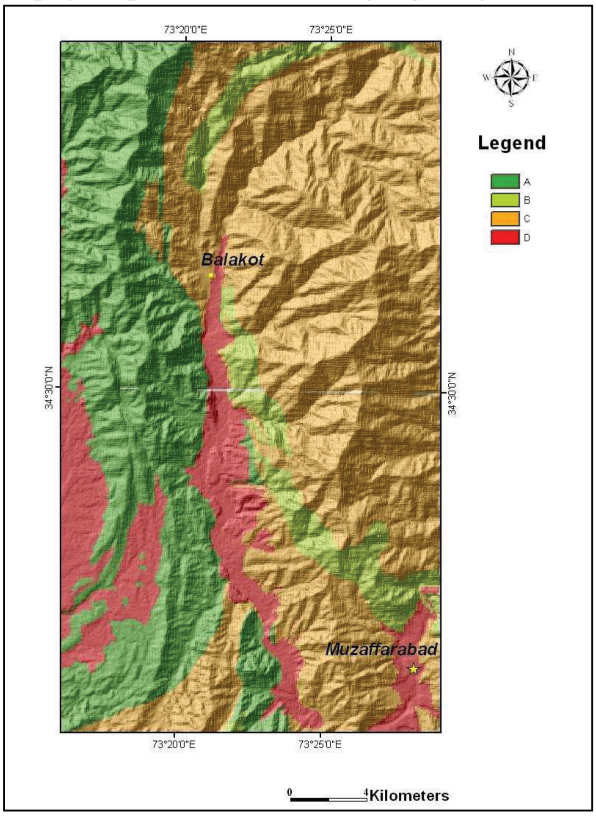

Figure 26 Site condition map based on geology and shear wave velocity

5. Conclusions and recommendations

5.4. Conclusions

The primary objective of the study was to predict the spatial distribution of regolith thickness by integrating field observations, lithology and topographic attributes and evaluate the impact of regolith thickness on seismic amplification using GIS Tools. This was accomplished under sub-objectives considered in the previous chapters. The following conclusions can be drawn based on the results discussed in the previous section.

- Thickness of regolith estimated by predicted regolith thickness map based on integration of field observations, lithology and topographic attributes varies from 1 to 10 meters the in the study area.
- The thickness is not evenly distributed and is related to slope, geology and elevation. This implies that the first hypothesis that the thickness of regolith is related to slope, geology and elevation is true. Thickness of regolith is more in the centre of the valleys and less to absent in the elevated areas depending upon the slope and geology of the site. High elevated areas marked by soft rocks have more cover of regolith than hard rocks at the same elevation.
- The impact of these surface features on thickness of regolith is slope > geology > elevation according to the Pearson correlation coefficients.
- The model derived from ASTER digital elevations models explains more variation and is more significant then that of SRTM digital elevations models.
- The second hypothesis that the Shear wave velocity from literature can be utilized for estimating the seismic response of an earthquake is utilized in preparing the site condition map based on geology and shear wave velocity. The shear wave velocity ranges from 180 to 1500 MHz.

5.5. Recommendations

- More data and predictors such as land use and soil map can be added for further studies.
- The geological map has some undivided units in Paleocene and Recent that were not devisable at 1:50,000. These units need to be differentiated for further refinement.

5.6. limitations

- The number of field measurements is limited and the models need to be validated.
- The measurements were taken mainly on the road sides, where the slopes were cut, measured depth of the unconsolidated material could be underestimated.

References

(AIJ), A.I.o.J., (JSCE), J.S.o.C.E. and (JGS), T.J.G.S., 2001. Report on the damage investigation of the 1999 Kocaeli earthquake in Turkey with the original data of the inventory survey on 2746 buildings. 4-8189-3250-7.

Aki, K. and Richards, P.G., 1980. Quantitative seismology. Freeman, San Francisco.

Anand, R.R. and Paine, M., 2002. Regolith geology of the Yilgarn Craton, Western Australia: implications for exploration. Australian Journal of Earth Sciences, 49(1): 3 - 162.

Ansal, A., 2004. Recent advances in earthquake geotechnical engineering and microzonation. Kluwer Academic, Dordrecht etc., 11 pp.

Aranha, P.R.A., Augustin, C.H.R.R. and Sobreira, F.G., 2002. The use of GPR for characterizing underground weathered profiles in the sub-humid tropics. Journal of Applied Geophysics, 49(4): 195-210.

Arcone, S.A. and Delaney, A.J., 1987. Airborne river-ice thickness profiling with helicopter-borne UHF short-pulse radar. Journal of Glaciology, 33(115): 330-340.

Aydan, O., 2006. Geological and seismological aspects of Kashmir earthquake of October 8, 2005 and geotechnical evaluation of induced failure of natural and cut slopes. Journal of the School of Marine Sciences and Technology, 4(1): 42.

Badaoui, M., Berrah, M.K. and Mebarki, A., 2009. Soil height randomness influence on seismic response: Case of an Algiers site. Computers and Geotechnics, 36(1-2): 102.

Bauer, R.A., Kiefer, J. and Hester, N., 2001. Soil amplification maps for estimating earthquake ground motions in the Central US. Engineering Geology, 62(1-3): 7.

Beauval, C., 2003. Quantification of frequency dependent lengthening of seismic ground motion due to local geology. Application to the Volvi Area, Greece. Bulletin of the seismological society of America 93(No 1).

Blumberg, D.G., Neta, T., Margalit, N., Lazar, M. and Freilikher, V., 2004. Mapping exposed and buried drainage systems using remote sensing in the Negev Desert, Israel. Geomorphology, 61(3-4): 239-250.

Borcherdt, R.D., 1970. Effects of local geology on ground motion near San Francisco Bay. Bull Seismol Soc Am, 69: 31.

Bullen, K.E., 1963. An introduction to the theory of seismology. Cambridge University Press, London.

CESNED, 2006. Earthquake hits Indonesia, Pakistan, Iran and Afghanistan., Cowasjee Earthquake Study Centre, NED University of Engineering and Technology, Department of Civil Engineering, Karachi, Pakistan, pp. 1.

Collins, M.E. and Doolittle, J.A., 1987. Using Ground-Penetrating Radar to Study Soil Microvariability. Soil Sci Soc Am, 51: 491-493.

Davis, J.L. and Annan, A.P., 1989. Ground-penetrating radar for high resolution mapping of soil and rock stratigraphy. Geophysical Prospecting, 37(5): 542.

Dehls, J.F., Olesen, Odleiv.,Olsen, Lars.,Harald Blikra, Lars., 2000. Neotectonic faulting in northern Norway; the Stuoragurra and Nordmannvikdalen postglacial faults. Quaternary Science Reviews, 19(14-15): 1447-1460.

Devkota, S., 2008. Parameterisation of soils properties for debris flow initiation modeling : a case study in the upper Tikovil river basin, Kerala, India, ITC, Enschede, 48 pp.

Dhakal, S., 2004. Empirical relations for earthquake response of slopes, ITC, Enschede, 74 pp.

Diego, L.P., Carlo, L. and Foti, S., 2004. Geophysical and geotechnical investigations for ground response analysis. In: A. Ansal (Editor), Recent advances in earthquake geotechnical engineeing and microzonation. Kluwer Academic Publishers, pp. 101.

Doolittle, J.A. and Collins, M.E., 1995. Use of soil information to determine application of ground penetrating radar. Journal of applied geophysics, 33(1-3): 101-108.

Doolittle, J.A. and Collins, M.E., 1998. A comparison of EM induction and GPR methods in areas of karst. Geoderma, 85(1): 83-102.

Ékes, C. and Hickin, E.J., 2001. Ground penetrating radar facies of the paraglacial Cheekye Fan, southwestern British Columbia, Canada. Sedimentary Geology, 143(3-4): 199-217.

Ellenkamp, G.R., 2004. Soil variability and landscape in the Machakos District, Kenya, Wageningen University, Wageningen.

Erdik, M. and Durukal, E., 2004. Strong ground motion. In: A. Ansal (Editor), Recent advances in earthquake geotechnical engineering and microzonation. Kluwer acadamic publishers, Paris, pp. 76.

Field, A., 2005. Discovering statistics using SPSS. Sage, London etc., 157 pp.

Fisher, E., McMechan, G.A. and Annan, P.A., 1992. Acquisition and processing of wide aperture ground penetrating radar data. J. Geophysics Res., 57(3): 495-504.
Fisher, E. et al., 1989. Determination of bedrock topography beneath the Greenland ice sheet by three-dimensional imaging of radar sounding data. J. Geophys. Res., 94: 2874-2882.
Freeland, R.S., Yoder, R.E. and Ammons, J.T., 1998. Mapping shallow underground features that influence site-specific agricultural production. Journal of Applied Geophysics, 40(1-3): 19-27.
Froese, D.G., Smith, D.G. and Clement, D.T., 2005. Characterizing large river history with shallow geophysics: Middle Yukon River, Yukon Territory and Alaska. Geomorphology, 67(3-4): 391-406.
Gazetteer, W., 2007. Pakistan: administrative divisions (population and area).
Gourry, J.-C., Vermeersch, F., Garcin, M. and Giot, D., 2003. Contribution of geophysics to the study of alluvial deposits: a case study in the Val d'Avaray area of the River Loire, France. Journal of Applied Geophysics, 54(1-2): 35-49.
Harari, Z., 1996. Ground-penetrating radar (GPR) for imaging stratigraphic features and groundwater in sand dunes. Journal of applied geophysics 36(1): 43-52.
Heimsath, A.M.E., Dietrich, W., Nishiizumi, K. and Finkel, R.C., 1999. Cosmogenic nuclides, topography, and the spatial variation of soil depth. Geomorphology, 27(1-2): 151-172.
Imai, T., Sakayama, T. and Kanemori, T., 1987. Use of ground penetrating radar and resistivity surveys for archaeological investigations. Geophysics, 52: 137–150.
Inglegton, J.E., 1999. Natural disaster management : a presentation to commemorate the international decade for natural disaster reduction IDNDR 1990 - 2000. Tudor Rose, Leicester, 53 pp.
Jakim, T.P., 1978. Seismic microzonation and related problems, The assessment and mitigation of earthquake risk. UNESCO
Paris, pp. 57.
Jol, H.M. and Bristow, C.S., 2003. GPR in sediments: advice on data collection, basic processing and interpretation, a good practice guide. In: Bristow, C.S., Jol, H.M. (Eds.), Ground-penetrating radar in sediments. Geological Society London, 211: 177–185.
Jørgensen, A.S. and Andreasen, F., 2007. Mapping of permafrost surface using ground-penetrating radar at Kangerlussuaq Airport, western Greenland. Cold Regions Science and Technology, 48(1): 64-72.
Kamp, U.G., Khattak., B.J., A., G. and Owen, L.A., 2008. GIS-based landslide susceptibility mapping for the 2005 Kashmir earthquake region. Geomorphology, In Press, Corrected Proof.
Kim, D.-S., Chung, C.-K., Sun, C.-G. and Bang, E.-S., 2002. Site assessment and evaluation of spatial earthquake ground motion of Kyeongju. Soil Dynamics and Earthquake Engineering, 22(5): 381.
Kung, K.-J.S., 1993. Using Ground-Penetrating Radar to Detect Layers of Discontinuous Dielectric Constant. Soil Sci Soc Am J(57): 335-340

Lawton, D. and Jol, H.M., 1994. Ground penetrating radar investigations of the Canada Creosote Site, Calgary. Can.Soc. Explor.Geophys., Rec., 13-18 April.
Mahajan, A.K., In Press. NEHRP soil classification and estimation of 1-D site effect of Dehradun fan deposits using shear wave velocity. Engineering Geology, Corrected Proof.
Mahajan, A.K. et al., 2007. Seismic microzonation of Dehradun City using geophysical and geotechnical characteristics in the upper 30 m of soil column. Journal of Seismology: 355-356.
Martinez, A. and Byrnes, A.P., 2001. Modeling Dielectric-constant values of Geologic Materials: An Aid to Ground-Penetrating Radar Data Collection and Interpretation. Current Research in Earth Sciences, Bulletin 247(part 1): 2.
Moorman, B.J., Robinson, S.D. and Burgess, M.M., 2003. Imaging periglacial conditions with ground-penetrating radar. Permafrost and Periglacial Processes., 14(4): 319–329.
Najman, Y., Pringle, M., Godin, L. and Olivers, G., 2002. A reinterpretation of the Balakot Formation: Implication for the tectonics of the NW Himalaya, Pakistan. TECTONICS,, 21(5).
Nascimento da Silva, C.C., de Medeiros, W.E., Jardim de Sá, E.F. and Neto, P.X., 2004. Resistivity and ground-penetrating radar images of fractures in a crystalline aquifer: a case study in Caiçara farm--NE Brazil. Journal of Applied Geophysics, 56(4): 295-307.
Nobes, D.C., 1999. Geophysical survey of burial sites: a case study of the Oaro Ururoa. Geophysics, 64(2): 357-367.
Olhoeft, G.R., 2008. Ground Penetrating Radar, Colorado.
Overgaard, T. and Jackobson, P.R., 2001. Mapping of glaciotectonic deformation in an ice marginal environment with ground penetrating radar. Journal of Applied Geophysics 47(3–4): 191–197.
Pakistan Water Gateway, J.R.K.F., 2007. .
Parasnis, D.S., 1997. Principles of applied geophysics. Chapman & Hall, London etc., 246 pp.

Pernito, M.A.E., 2008. Rock mass slope stability analysis based on 3D terrestrial laser scanning and ground penetrating radar, ITC, Enschede, 40 pp.
Petersen, M., W., Bryant, C., Cramer, M., Reichle. and Real, C., 1997. Seismic ground-motion hazard mapping incorporating site effects for Los Angeles, Orange, and Ventura counties, California. Bull. Seism. Soc. Am, 87: 249–255.
Pitilakis, K., 2004. Site effects. In: A. Ansal (Editor), Recent advances in earthquake geotechnical engineering. Kluwer academy.
Rayhani, M., El Naggar, M. and Tabatabaei, S., 2008. Nonlinear Analysis of Local Site Effects on Seismic Ground Response in the Bam Earthquake. Geotechnical and Geological Engineering, 26(1): 91.
Remondo, J., González-Díez, A., De Terán, J.R.D. and Cendrero, A., 2003. Landslide Susceptibility Models Utilising Spatial Data Analysis Techniques. A Case Study from the Lower Deba Valley, Guipuzcoa (Spain). Natural Hazards, 30(3): 267-279.
Sabbar, A.S., 2009. Application of ground penetrating radar (GPR) in detection of ground water table.
Sapkota, R., 2008. Modelling runoff and erosion in Namchun watershed, Thailand, ITC, Enschede, 19 pp.
Sass, O., 2007. Bedrock detection and talus thickness assessment in the European Alps using geophysical methods. Journal of Applied Geophysics, 62(3): 254-269.
Sass, O., Bell, R.,Glade, T., 2008. Comparison of GPR, 2D-resistivity and traditional techniques for the subsurface exploration of the Öschingen landslide, Swabian Alb (Germany). Geomorphology, 93(1-2): 89-103.
Sass, O. and Krautblatter, M., 2007. Debris flow-dominated and rockfall-dominated talus slopes: Genetic models derived from GPR measurements. Geomorphology, 86(1-2): 176-192.
Shafique, M., 2008. Predicting topographic aggravation of seismic ground shaking using geospatial tools : a case study of Kashmir earthquake, Pakistan, ITC, Enschede, 7 pp.
Sharma, P.V., 1997. Environmental and engineering geophysics. Cambridge University Press, Cambridge etc., 475 pp.
Smemoe, C.M., 2000. Processing and visualization of ground penetrating radar data for assessing natural hydrologic conditions, Brigham young university.
Srbulov, M., 2009. Soil Properties, Geotechnical Earthquake Engineering, pp. 13.
Stephan, G. and Florian, L., **1996**. Application of ground penetrating radar in glaciology and perrmafrost prospecting, Arctic centre, Finland.
Sternberg, B.K. and McGill, J.W., 1995. Archaeology studies in southern Arizona using ground penetrating radar. Journal of Applied Geophysics, 33(1): 209-225(17).
Stoltman, J.P.E., Lidstone, J.E. and Dechano, L.M.E., 2004. International perspectives on natural disasters : occurrence, mitigation and consequences. Advances in natural and technological hazards research, 21. Kluwer Academic, Dordrecht etc., 11 pp.
Stove, G.C. and Addyman, P.V., 1989. Ground probing pulse radar:an experiment in archeological remote sensing. Antiquity, 63: 337-342.
Tirén, S.A. and Wänstedt, S., Sträng, T., 2001. Moredalen -- a canyon in the Fennoscandian Shield and its implication on site selection for radioactive waste disposal in south-eastern Sweden. Engineering Geology, 61(2-3): 99-118.
Torres Acosta, C.A., 2008. Geometric characterization of rock mass discontinuities using terrestrial laser scanner and ground penetrating radar, ITC, Enschede, 74 pp.
Tucker, B.E.E., Erdik, M.E. and Hwang, C.N.E., 1994. Issues in urban earthquake risk. NATO ASI Series E: Applied Sciences, 271. Kluwer Academic, Dordrecht etc., 11 pp.
Vaughan., C.J., 1986. Ground-penetrating radar surveys used in archaeological investigations. Geophysics, 51(595).
Wechsler, S.P., 2006. Digital Elevation Model (DEM) Uncertainty: Evaluation and Effect on Topographic Parameters.
Weinstein, E., Mina., Beck, A. and Ezersky, M., 2003. Geophysical investigations in the service of Mount Carmel (Israel) prehistoric research. Journal of Archaeological Science, 30(10): 1331-1341.
Wills, C.J. et al., 2000. A site condition map for California based on geology and shear wave velocity Bulletin of the Seismological Society of America, 90(6B): 187-208.
Yang, J. and Yan, X.R., 2009. Site response to multi-directional earthquake loading: A practical procedure. Soil Dynamics and Earthquake Engineering, 29(4): 710.
Young, R.A. and Sun, J., 1999. Revealing stratigraphy in ground-penetrating radar data using domain filtering. Geophysics 64: 435-442.

Appendix 1:

Results of Ground Penetrating Radar

6.1. Introduction

Ground Penetrating Radar (GPR) is a non invasive geophysical method for probing beneath the surface of the earth. It utilizes a very short burst of radio-frequency energy in the frequency band of 10-1000 MHz, radiated into the ground to detect discontinuities in dielectric properties (Aranha et al., 2002). There are four components of GPR i.e. the transmitting unit, the receiving unit, the control unit and the display unit (Davis and Annan, 1989). The GPR system computes the time of the pulse which it takes to travel from transmitting antenna to the receiving antenna after being reflected or refracted from the subsurface (figure 27). When radar pulse travels in subsurface part of it is reflected depending on the electrical properties of the subsurface material in the form of peaks which are augmented, digitized and processed for display in the display unit (Smemoe, 2000).

The radars are of different types e.g. pulse radar that emits pulses of electromagnetic waves and the frequency modulated sine wave or holographic radar which depend on the mapping of spatial distribution of scattered waves (Parasnis, 1997). Pulse radars are commonly used for ground investigations and are grouped under the name of ground penetrating radar or GPR. They have found extensive use in the fields of geology, engineering, environmental studies, hydrology, archaeology, glaciology and forensics.

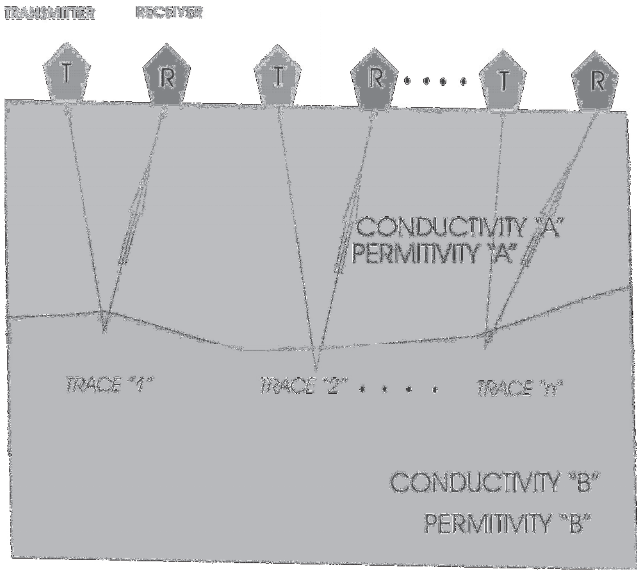

Figure 27 The principle of operation of GPR

6.2. GPR Theory

There are two basic modes of GPR profiling, one with the fixed antenna separation called reflection profiling and second with variable distance of the antennas like CMP (Sabbar, 2009). The basic principles of GPR are discussed by Olhoeft (2008).The propagation of radar signal depends on the high frequency electrical properties of the ground as they dominate the conductive properties of many geological materials at such high frequencies. Radar signal velocity in most of the low loss, nonmagnetic geological materials as is as follows (Sharma, 1997).

$$V = c / \sqrt{(\mu r\ \varepsilon r)} \qquad \textbf{Equation 10}$$

Where V is the radar velocity, μr is the relative magnetic permeability of the medium, εr is the relative dielectric permittivity of the medium and c (3 x108 m/s) is the velocity of EM waves in free space.

The resolution is ability of the system to distinguish two signals that are close to each other. The resolution will increase with increase in resolution but the depth of penetration will decrease (Stephan and Florian, 1996). The depth of penetration is mainly controlled by conductivity 'σ' as the magnetic permeability is almost unity and the dielectric permittivity doesn't vary more than a factor 10. The relation is shown by the equation 10.

$$\delta = (2/\sigma) \sqrt{(\varepsilon/\mu} \qquad \textbf{Equation 11}$$

Bulk dielectric constants of common earth materials are given in table 9.

Table 9 Bulk dielectric constants (measured at 100 MHz) of common earth materials: Source (Martinez and Byrnes, 2001)

Material	**(Davis and Annan, 1989)**	**(Daniels , 1996)**
Air	1	1
Distilled water 80	80	
Fresh water	80	81
Sea water	80	
Fresh water ice	3-4	4
Sea water ice		4-8
Snow		8-12
Permafrost		4–8
Sand, dry	3–5	4–6
Sand, wet	20–30	10–30
Sandstone, dry		2–3
Sandstone, wet		5–10
Limestone	4–8	
Limestone, dry		7
Limestone wet		8
Shale	5–15	
Shale, wet		6–9
Silts	5–30	
Clays	5–40	
Clay, dry		2–6
Clay, wet		15–40
Soil, sandy dry		4–6
Soil, sandy wet		15–30
Soil, loamy dry		4–6
Soil, loamy wet		10–20
Soil, clayey dry		4–6
Soil, clayey wet		10–15
Coal, dry		3.5
Coal, wet		8
Granite	4–6	

Granite, dry		5
Granite, wet		7
Salt, dry	5–6	4–7

6.3. GPR Application

Previously, GPR's have been applied in the fields of stratigraphic mapping (Davis and Annan 1989; (Davis and Annan, 1989; Dehls, 2000; Ékes and Hickin, 2001; Fisher et al., 1992; Froese et al., 2005; Gourry et al., 2003; Sass, 2007; Sass, 2008; Sass and Krautblatter, 2007; Torres Acosta, 2008; Young and Sun, 1999) Torres Acosta 2008), determination of permafrost thickness (Arcone and Delaney, 1987; Fisher et al., 1989; Jørgensen and Andreasen, 2007), environmental contamination (Davis and Annan, 1989; Lawton and Jol, 1994; Tirén and Wänstedt, 2001), archaeology (Blumberg et al., 2004; Imai et al., 1987; Nobes, 1999; Sternberg and McGill, 1995; Stove and Addyman, 1989; Vaughan., 1986; Weinstein et al., 2003), groundwater (Harari, 1996; Nascimento da Silva et al., 2004) and the determination of soil aspects (Collins and Doolittle, 1987; Doolittle and Collins, 1995; Doolittle and Collins, 1998; Freeland et al., 1998; Kung, 1993).

6.4. Data processing

GPR data is processed before interpretation and visualization in order to attain a representative image. The details of data processing can be found in the studies by Pernito (2008). In the present study air wave and ground wave were used for the calculation of finding the depth of the reflection from bedrock therefore background removal was also not applied. Automatic gain control (AGC) was only used to compensate for possible damping and geometric spreading losses.

6.5. GPR application in delineating soil bedrock boundary.

In the present study the frequency of 50 MHz was used to find the depth of soil bedrock boundary because of the depth of penetration in the soil and rocks of the study area. This was also confirmed by a previous study by Sass and Krautblatter (2007), which found this frequency suitable for bedrock study. There are many varities of GPR's like road cart that can be towed behind a car and others but due to the rugged topography, rough terrain type antennas with 2 m interval were used as shown in the figure 28.

__Figure 28 Rough terrain type GPR being used in the field.__

Radar facies (Jol and Bristow, 2003; Moorman et al., 2003; Overgaard and Jackobson, 2001), which are textural patterns; continuity and strength of reflections typical for certain sediments can help in distinguishing subsurface units. The radar gram obtained from the field is shown in the figure 29.

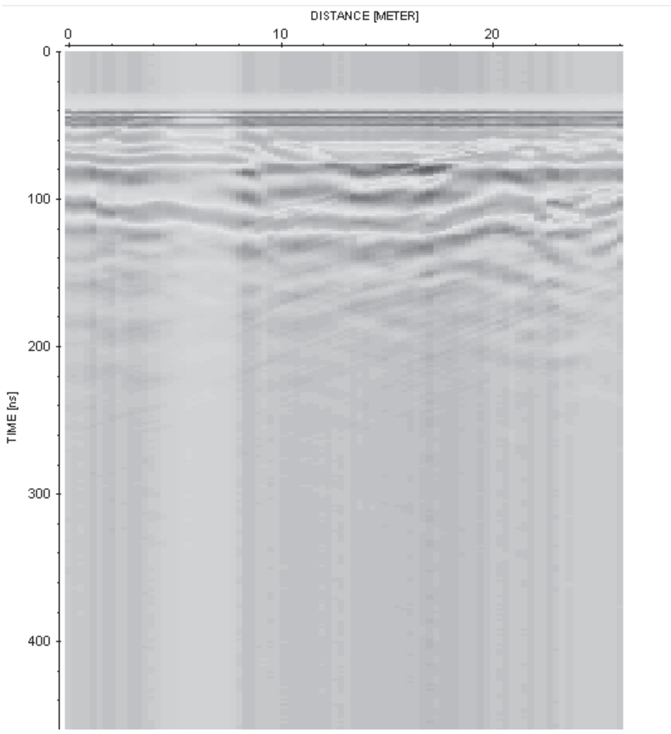

Figure 29 Radar gram obtained from the field